© 2014. Published by The Company of Biologists Ltd | Journal of Cell Science (2014) 127, 5204–5217 doi:10.1242/jcs.150961

RESEARCH ARTICLE

# Proteasome dysfunction induces muscle growth defects and protein aggregation

**Yasuo Kitajima[1,2,§], Yoshitaka Tashiro[3,‡,§], Naoki Suzuki[1,*,§,¶], Hitoshi Warita[1], Masaaki Kato[1], Maki Tateyama[1], Risa Ando[1], Rumiko Izumi[1], Maya Yamazaki[4], Manabu Abe[4], Kenji Sakimura[4], Hidefumi Ito[5], Makoto Urushitani[3], Ryoichi Nagatomi[2], Ryosuke Takahashi[3] and Masashi Aoki[1,¶]**

## ABSTRACT

The ubiquitin–proteasome and autophagy–lysosome pathways are the two major routes of protein and organelle clearance. The role of the proteasome pathway in mammalian muscle has not been examined *in vivo*. In this study, we report that the muscle-specific deletion of a crucial proteasomal gene, *Rpt3* (also known as *Psmc4*), resulted in profound muscle growth defects and a decrease in force production in mice. Specifically, developing muscles in conditional *Rpt3*-knockout animals showed dysregulated proteasomal activity. The autophagy pathway was upregulated, but the process of autophagosome formation was impaired. A microscopic analysis revealed the accumulation of basophilic inclusions and disorganization of the sarcomeres in young adult mice. Our results suggest that appropriate proteasomal activity is important for muscle growth and for maintaining myofiber integrity in collaboration with autophagy pathways. The deletion of a component of the proteasome complex contributed to myofiber degeneration and weakness in muscle disorders that are characterized by the accumulation of abnormal inclusions.

**KEY WORDS: Proteasome, Autophagy, Skeletal muscle, Muscle atrophy**

## INTRODUCTION

The ubiquitin–proteasome and autophagy–lysosome pathways are the two major routes for protein and organelle clearance in cells (Braun and Gautel, 2011). These two systems are controlled by a transcriptional program that upregulates several crucial and rate-limiting enzymes (Glass, 2010; Jagoe and Goldberg, 2001). Proteasomal proteolysis is important in several organs; for example, proteasome inhibition using MG-132 leads to the cytoplasmic aggregation of TAR DNA-binding protein 43 (TDP-43) in cultured hippocampal and cortical neurons and in immortalized motor neurons (van Eersel et al., 2011). Similarly, the depletion of the 26S proteasome in mouse brain neurons causes neurodegeneration (Bedford et al., 2008).

The loss of skeletal muscle mass in humans at an older age, which is called sarcopenia, is a rapidly growing health issue worldwide (Vellas et al., 2013). The regulation of skeletal muscle mass largely depends on protein synthesis and degradation processes. Two muscle-specific E3 ubiquitin ligases, muscle RING finger 1 (MuRF1, also known as TRIM63) and muscle atrophy F-Box (MAFbx, also known as atrogin-1 or FBXO32), are thought to be key regulators of proteasomal proteolysis in skeletal muscle, especially under atrophy-inducing conditions (Cai et al., 2004; Sandri et al., 2004; Stitt et al., 2004). These proteins are markers of muscle atrophy because they are expressed at relatively low levels in resting muscle but are upregulated under a variety of atrophy-inducing conditions. The dysregulation of the proteasome system is also involved in several muscle diseases. Members of the ubiquitin-proteasome system are upregulated and the global ubiquitylation of proteins is increased in the muscles of dystrophic patients with laminin α2 chain deficiency. Interestingly, proteasome inhibition using MG-132 significantly improved the dystrophic phenotype (Carmignac et al., 2011). MG-132 also improves the dystrophic phenotype in a model of dystrophin deficiency (Bonuccelli et al., 2003; Winder et al., 2011). Therefore, the upregulation of proteasomal proteolysis likely leads to a reduction in skeletal muscle mass, which is in contrast to animal models of proteasomal dysfunction or downregulation in brain neurons that leads to degeneration. We hypothesized that the findings using MG-132 might involve proteasomal inhibition in non-muscle cells in the tissue. Because muscular dystrophy is characterized by inflammation, the effect of MG-132 on inflammatory cells must be considered.

Autophagy is another important cellular pathway for protein and organelle degradation. The efficiency of autophagic degradation declines during aging, leading to the accumulation of intracellular waste products (Salminen and Kaarniranta, 2009). Autophagy is an evolutionarily conserved degradative pathway through which long-lived intracellular proteins and organelles are delivered to the lysosome for destruction. This pathway is involved in the cellular response to starvation, cellular differentiation, cellular death, aging, cancer and neurodegenerative disease (Todde et al., 2009). The excessive activation of autophagy aggravates muscle wasting (Zhao et al.,

[1]Department of Neurology, Tohoku University School of Medicine, 1-1 Seiryo-machi, Aoba-ku, Sendai 980-8574, Japan. [2]Department of Medicine and Science in Sports and Exercise, Tohoku University Graduate School of Medicine, 1-1 Seiryo-machi, Aoba-ku, Sendai 980-8574, Japan. [3]Department of Neurology, Kyoto University Graduate School of Medicine, Kyoto 606-8501, Japan. [4]Niigata University, Department of Cellular Neurobiology Brain Research Institute, Niigata 951-8510, Japan. [5]Department of Neurology, Wakayama Medical University Graduate School of Medicine, Wakayama 641-8510, Japan.
*Present Address: Department of Stem Cell and Regenerative Biology, Harvard University, Cambridge MA 02138, USA. ‡Present Address: SK Project, Medical Innovation Center, Kyoto University. Kyoto University Graduate School of Medicine, Kyoto 606-8501, Japan.
§These authors contributed equally to this work

¶Authors for correspondence (naoki@med.tohoku.ac.jp; aokim@med.tohoku.ac.jp)

This is an Open Access article distributed under the terms of the Creative Commons Attribution License (http://creativecommons.org/licenses/by/3.0), which permits unrestricted use, distribution and reproduction in any medium provided that the original work is properly attributed.

**Received 2 February 2014; Accepted 1 September 2014**





Journal of Cell Science

Journal of Cell Science (2014) 127, 5204–5217 doi:10.1242/jcs.150961

2007). Interestingly, a study using mice with a muscle-specific deletion of *Atg7* revealed the upregulation of MuRF1 and atrogin-1, suggesting crosstalk between the autophagy and proteasomal pathways in skeletal muscle (Masiero et al., 2009). Proteasomal inhibition generally induces autophagy (Ding et al., 2007). Therefore, the role of the proteasomal pathway in skeletal muscle homeostasis should be evaluated while also considering autophagy and protein synthesis activity; however, the effect of proteasomal downregulation on autophagy using a loss-of-function strategy has not yet been described.

Proteasomal degradation is mediated by an ATP-dependent protease complex, the 26S proteasome, which is present in both the cytoplasm and nucleus. The 26S proteasome consists of a proteolytic, cylinder-shaped particle (the 20S proteasome) and an ATPase-containing complex (the 19S cap complex). The 19S cap complex unfolds ubiquitin-conjugated proteins to allow their entry into the 20S cylindrical particle. The 19S complex contains several putative ATPases, such as PSMC1–PSMC6. These subunits form a large family with a highly conserved ATPase domain (Sakao et al., 2000). PSMC4, also known as Rpt3, is an essential subunit of the 26S proteasome and is required for the degradation of most proteasomal substrates. In particular, Rpt3-deficient mice die before implantation owing to a defect in blastocyst development (Sakao et al., 2000). Interestingly, an insertion/deletion variant in intron 5 of the *Rpt3* gene was frequently found in a cohort of patients with Parkinson's disease (Marx et al., 2007). The combined knockdown of both *Rpt3* and *Rpt6* caused defects in the assembly of regulated particles of the proteasome and led to diminished peptidase activity in HEK293T cells (Kaneko et al., 2009). Recently, we reported that the conditional knockout of the proteasome subunit *Rpt3* in motor neurons caused locomotor dysfunction that was accompanied by progressive motor neuron loss and gliosis in mice (Tashiro et al., 2012). Thus, the specific deletion of Rpt3 in skeletal muscle tissue might provide a better understanding of the role of the proteasome in muscle homeostasis without affecting other cell types in the tissue.

The working hypothesis of this study was that the downregulation of the ubiquitin proteasomal pathway might attenuate myocellular catabolic pathways to favor the maintenance of skeletal muscle mass. Thus, we generated conditional *Rpt3*-knockout mice to specifically block proteasomal activity in skeletal muscle to clarify the role of the proteasomal system in skeletal muscle tissue. Additionally, because the dysregulation of autophagy is involved in the pathogenic mechanisms of several myopathies, such as Pompe disease (Raben et al., 2008), Danon disease (Nishino et al., 2000), VMA21 deficiency (Ramachandran et al., 2013), autosomal dominant inclusion body myopathy associated with Paget's disease of the bone and frontotemporal dementia with valosin-containing protein (VCP) mutation (Watts et al., 2004), GNE myopathy (Li et al., 2013) and collagen VI muscular dystrophy (Grumati et al., 2010), we also investigated morphologically similar anomalies using specific immunohistochemical markers of known myopathies in the conditional *Rpt3*-knockout mice.

## RESULTS

### Generation of muscle-specific Rpt3-knockout mice

Rpt3-flox/flox mice were generated at Kyoto University, as described previously (Tashiro et al., 2012). Floxed Rpt3 mice (Rpt3-f/f) were crossed with a transgenic line expressing Cre recombinase under the control of a skeletal-muscle actin (ACTA1) promoter (Miniou et al., 1999) to generate muscle-specific Rpt3-knockout mice. However, an ACTA1-Cre-positive Rpt3-f/f mouse was not successfully generated when genotyping was performed in the F2 generation at 4 weeks of age. The examination of E18.5 embryo genotypes revealed ACTA1-Cre/Rpt3-f/f embryos, suggesting that this genotype causes embryonic lethality.

Rpt3-f/f mice were then crossed with a transgenic line expressing Cre recombinase under the control of a myosin light chain 1 fast (Mlc1f, also known as Myl1) promoter to generate muscle-specific Rpt3-knockout mice, hereafter referred to as $Rpt3^{-/-}$ mice (Fig. 1A). Mlc1f-Cre/$Rpt3^{+/+}$ mice were used as controls and are herein referred to as $Rpt3^{+/+}$ mice (Fig. 1A). In Mlc1f-Cre mice, Cre activity was detected in skeletal muscle tissue, including the gastrocnemius, tibialis anterior and soleus muscles, but not in the heart (Bothe et al., 2000). *Mlc* transcripts are initially detected between E8.5 and E9.5 and are expressed robustly beginning at E10.5 (Mourkioti et al., 2008). Mlc1f expression is restricted to fast-twitch fibers in adults (Lyons et al., 1990), in contrast to the ACTA1 promoter, which becomes active in both the skeletal muscle and heart beginning at E9.5 (Miniou et al., 1999). Accordingly, Rpt3 protein was only slightly detectable in the gastrocnemius muscles, in which fast-twitch fibers predominate, of homozygous mice (Fig. 1B). Rpt3 protein was also markedly decreased in the soleus muscle (Fig. 1B). Mlc1f-promoter-driven Cre has an excision efficiency of 40–50% according to Southern blot analysis (Bothe et al., 2000). The trace amounts of persistent Rpt3 protein expression might therefore reflect non-excised floxed Rpt3. However, the presence of slow-twitch muscle fibers, endothelial cells, fibroblasts, macrophages, blood cells and mesenchymal cells might also contribute to the remaining expression. An immunoblotting analysis demonstrated multiple ladder bands bound by anti-Rpt3 (data not shown). The specificity of the Rpt3 antibody used was not high enough to obtain an Rpt3-specific immunohistochemical image.

### Proteasomal inhibition induces muscle growth defects and the loss of force production

The appearance of the resultant $Rpt3^{-/-}$ mice was distinct from that of age-matched control $Rpt3^{+/+}$ mice (Fig. 1C); $Rpt3^{-/-}$ mice exhibited kyphosis and a smaller body frame. The growth curve showed a severe reduction in body growth, which differed from that of controls beginning at 3 weeks of age (Fig. 1D), whereas the survival curve suggested that the $Rpt3^{-/-}$ mice had a reduced lifespan (Fig. 1E). Skeletal muscles also appeared smaller in the $Rpt3^{-/-}$ mice (Fig. 1F); the absolute weights of the tibialis anterior, gastrocnemius and soleus muscles were smaller in $Rpt3^{-/-}$ mice at 4 weeks of age (Fig. 1G). However, when muscle weight was evaluated per body weight, virtually no difference was detected between $Rpt3^{+/+}$ and $Rpt3^{-/-}$ animals in the soleus muscle, which is >50% slow-twitch fibers, whereas larger differences in fast-twitch-dominant muscles were observed between the animals (Fig. 1H). Additionally, the average heart weight was similar in both $Rpt3^{-/-}$ and $Rpt3^{+/+}$ mice (Fig. 1I), most likely because the Mlc1f promoter is not active in the heart.

The grasping strength of $Rpt3^{-/-}$ mice was significantly lower than that of $Rpt3^{+/+}$ mice, most likely because of the decreased muscle mass (Fig. 1J). Furthermore, creatine kinase levels were increased in $Rpt3^{-/-}$ mice, suggesting the presence of muscle damage in the mutant mice (Fig. 1K). $Rpt3^{-/-}$ mice also demonstrated a waddling gait, and their step lengths were markedly shorter compared with those of $Rpt3^{+/+}$ mice (Fig. 1L).

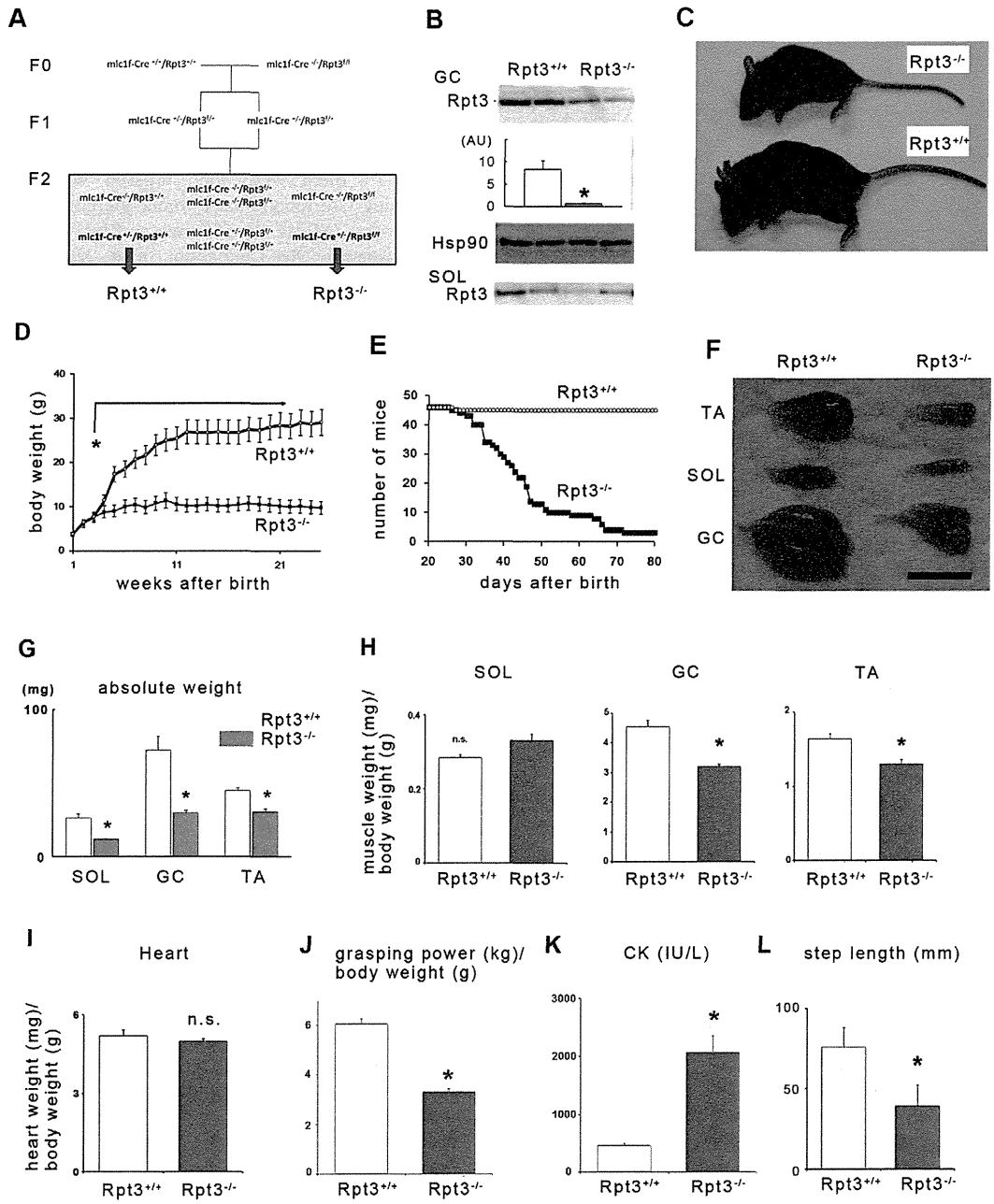


**Fig. 1. Phenotypes of muscle-specific Rpt3-knockout mice.** (A) Generation of the Rpt3$^{-/-}$ mice. Mlc1f-Cre$^{+/-}$/Rpt3$^{f/-}$ mice were mated to produce mlc1f-Cre$^{+/-}$/Rpt3$^{+/+}$ mice and mlc1f-Cre$^{+/-}$/Rpt3$^{f/f}$ mice (referred to as Rpt3$^{+/+}$ mice and Rpt3$^{-/-}$ mice, respectively). (B) Muscle homogenates were immunoblotted with antibodies against Rpt3 and Hsp90. Rpt3 protein was nearly undetectable in the homogenate of gastrocnemius (GC) from Rpt3$^{-/-}$ mice. The homogenate from soleus muscle gave a similar result. Quantitative data are also presented ($n$=3). White bar, Rpt3$^{+/+}$ mice; gray bar, Rpt3$^{-/-}$ mice. SOL, soleus; AU, arbitrary units. (C) The general appearance of Rpt3$^{-/-}$ mice is shown. Note the smaller body frame and kyphosis in Rpt3$^{-/-}$ mice. (D) The body weights of Rpt3$^{+/+}$ and Rpt3$^{-/-}$ mice are shown ($n$=10 and 11, respectively). Note that the difference in the body weight became prominent after 3 weeks of age. Open circles, Rpt3$^{+/+}$; closed squares, Rpt3$^{-/-}$. (E) Kaplan–Meier survival curves for Rpt3$^{+/+}$ and Rpt3$^{-/-}$ mice ($n$=46 each). (F) Appearance of excised skeletal muscles of Rpt3$^{+/+}$ and Rpt3$^{-/-}$ mice. TA, tibialis anterior. Scale bar: 1 cm. (G) Absolute skeletal muscle weight (mg) was significantly different between Rpt3$^{+/+}$ and Rpt3$^{-/-}$ mice in tibialis anterior, gastrocnemius and soleus muscles ($n$=10). White bars, Rpt3$^{+/+}$; gray bars, Rpt3$^{-/-}$. (H) Skeletal muscle weight (mg)/body weight (g) were significantly different between Rpt3$^{+/+}$ and Rpt3$^{-/-}$ mice in tibialis anterior and gastrocnemius muscles (mostly fast-twitch fibers) but not in soleus muscle (half of the fibers are slow-twitch) ($n$=10). (I) Heart weight (mg)/body weight (g) was not significantly altered in the Rpt3$^{-/-}$ mice. (J) Grasping power (kg)/body weight (g) was significantly lower in the Rpt3$^{-/-}$ mice ($n$=5). (K) Creatine kinase (CK; IU/l) was significantly higher in the Rpt3$^{-/-}$ mice ($n$=5). (L) The step length (mm) was significantly shorter in Rpt3$^{-/-}$ mice compared with Rpt3$^{+/+}$ mice ($n$=5). Quantitative data show the mean+s.e.m.; *$P$<0.05; n.s., non-significant [Student's $t$-test (B,G–I,K,L); Mann–Whitney U test (J)].





Journal of Cell Science

Journal of Cell Science (2014) 127, 5204–5217 doi:10.1242/jcs.150961

### Morphological features of skeletal muscle in Rpt3$^{-/-}$ mice

The examination of the skeletal muscle morphology in Rpt3$^{-/-}$ mice revealed degenerative changes, the accumulation of basophilic inclusions in muscle fibers and centrally nucleated myofibers at 4 weeks of age (Fig. 2A). Mononuclear cell infiltration around muscle fibers was also observed (Fig. 2A). The myofiber cross-sectional area was decreased in Rpt3$^{-/-}$ mice (Fig. 2B), indicating muscle fiber atrophy. As expected, fast-twitch muscle fibers were severely atrophied, whereas the average diameters of the slow-twitch fibers were approximately the same in both Rpt3$^{+/+}$ and Rpt3$^{-/-}$ mice (Fig. 2C,D). These findings indicate that the phenotypic change results from the deletion of the proteasomal component Rpt3 specifically in fast-twitch muscle fibers. In addition, the proportion of slow-twitch fibers was greater in the gastrocnemius muscle of Rpt3$^{-/-}$ mice, which is most likely due to the degeneration of Rpt3-deficient fast-twitch fibers (Fig. 2E).

Next, the muscle tissue from the fast-twitch-dominant tibialis anterior muscle of Rpt3$^{-/-}$ mice was examined by electron microscopy. The myofibrils in Rpt3$^{-/-}$ mice were smaller in diameter than those in Rpt3$^{+/+}$ mice (Fig. 2F,G). The distension of the sarcoplasmic reticulum and enlarged interstitial spaces were observed in Rpt3$^{-/-}$ skeletal muscle tissue (Fig. 2F,G). In a subset of the muscle fibers, the distension of the sarcoplasmic reticulum (Fig. 2H,I) as well as vesicle formation and ruptured membranes were observed (Fig. 2I). In addition, a comparison of the electron micrographs obtained from the tibialis anterior muscles of Rpt3$^{-/-}$ and Rpt3$^{+/+}$ mice did not demonstrate increases in the number of autophagosomes and autolysosomes.

Furthermore, no marked defect or reduction in dystrophin or the components of the dystrophin–glycoprotein complex was observed (Fig. 3A,B). No apparent differences were observed in α1-syntrophin, α-dystroglycan, α-sarcoglycan, aquaporin-4, β-sarcoglycan, dystrophin, dysferlin, neuronal nitric oxide

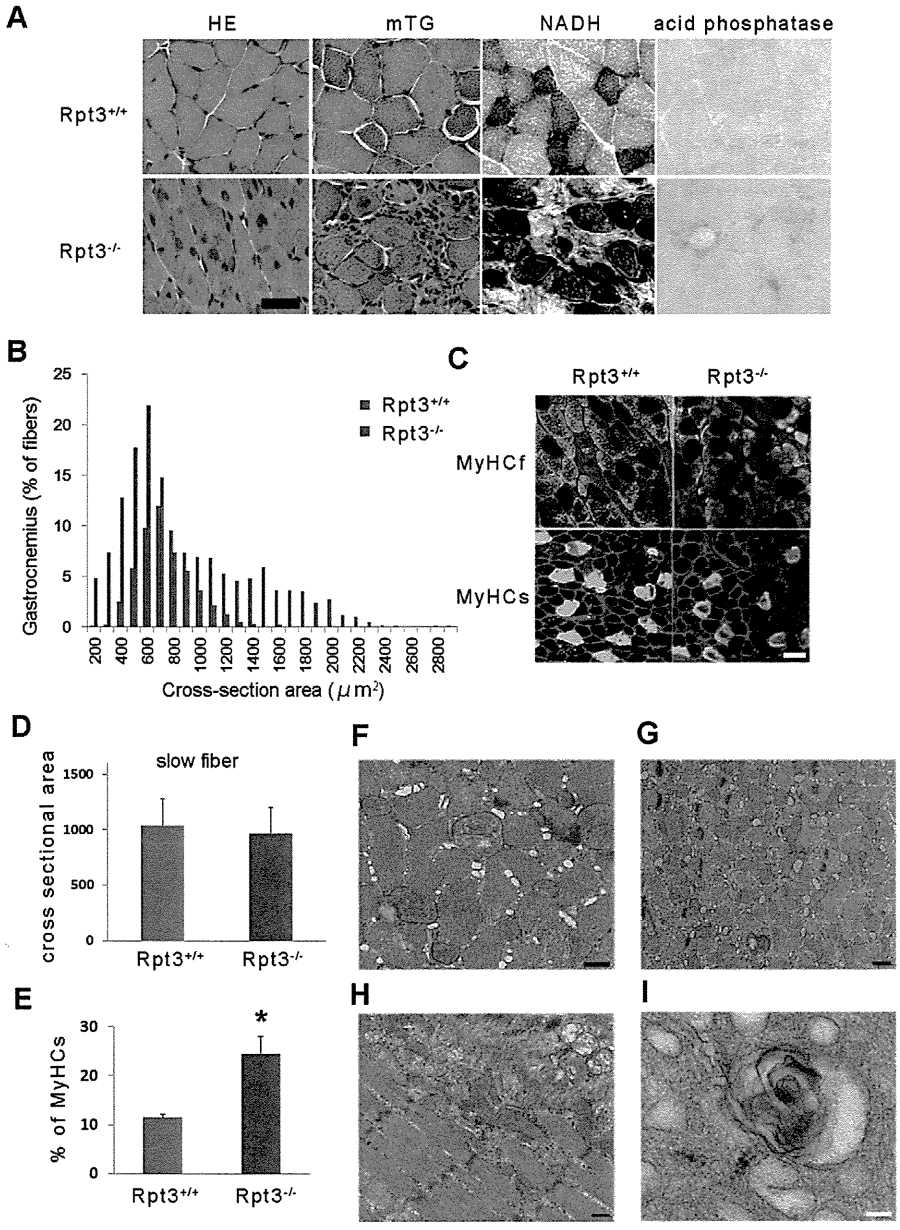


**Fig. 2. Morphological changes in the muscles of Rpt3$^{-/-}$ mice.** (A) Hematoxylin and eosin (HE) staining shows a general decrease in myofiber size along with the presence of central nuclei, basophilic inclusions and vacuolated fibers in the gastrocnemius of Rpt3$^{-/-}$ mice at 4 weeks of age. Modified trichrome Gomori (mTG) staining revealed several basophilic inclusions in the myofibers and monocellular infiltrations in the interstitial perimysial space in Rpt3$^{-/-}$ mice. NADH staining suggested that the myofibrils were disorganized in Rpt3$^{-/-}$ mice. Acid phosphatase staining revealed mononuclear cell infiltrations around muscle fibers in Rpt3$^{-/-}$ mice. Scale bar: 50 μm. (B) Quantification of the cross-sectional area of the myofibers in the gastrocnemius of Rpt3$^{-/-}$ mice and Rpt3$^{+/+}$ mice ($n$=5). $P$<0.05 (Student's $t$-test). (C) Immunohistochemistry using myosin heavy chain slow (MyHCs) and fast (MyHCf) in the gastrocnemius of Rpt3$^{-/-}$ and Rpt3$^{+/+}$ mice. The diameter of the MyHCf-positive fibers in Rpt3$^{-/-}$ mice was smaller; however, the same was not observed for the MyHCs-positive fibers. Red, laminin; green, MyHCf or MyHCs. Scale bar: 50 μm. (D) Quantitative data are also shown from the gastrocnemius of Rpt3$^{-/-}$ and Rpt3$^{+/+}$ mice ($n$=200 for each fiber type). (E) The percentage of slow-twitch fibers was increased in the gastrocnemius of Rpt3$^{-/-}$ and Rpt3$^{+/+}$ mice ($n$=5). Quantitative data show the mean+s.e.m.; *$P$<0.05 (Student's $t$-test). (F–I) Electron microscopy findings in the tibialis anterior muscles. Axial (F,G) and longitudinal (H,I) sections from 6-week-old Rpt3$^{+/+}$ mice (F) and Rpt3$^{-/-}$ mice (G–I). The myofibrils were smaller and the interstitial space was wider in the Rpt3$^{-/-}$ mice. Sarcoplasmic reticulum dilation, filamentous structures and vacuolated structures were observed (H,I). Scale bars: 500 nm.

Journal of Cell Science

Journal of Cell Science (2014) 127, 5204–5217 doi:10.1242/jcs.150961

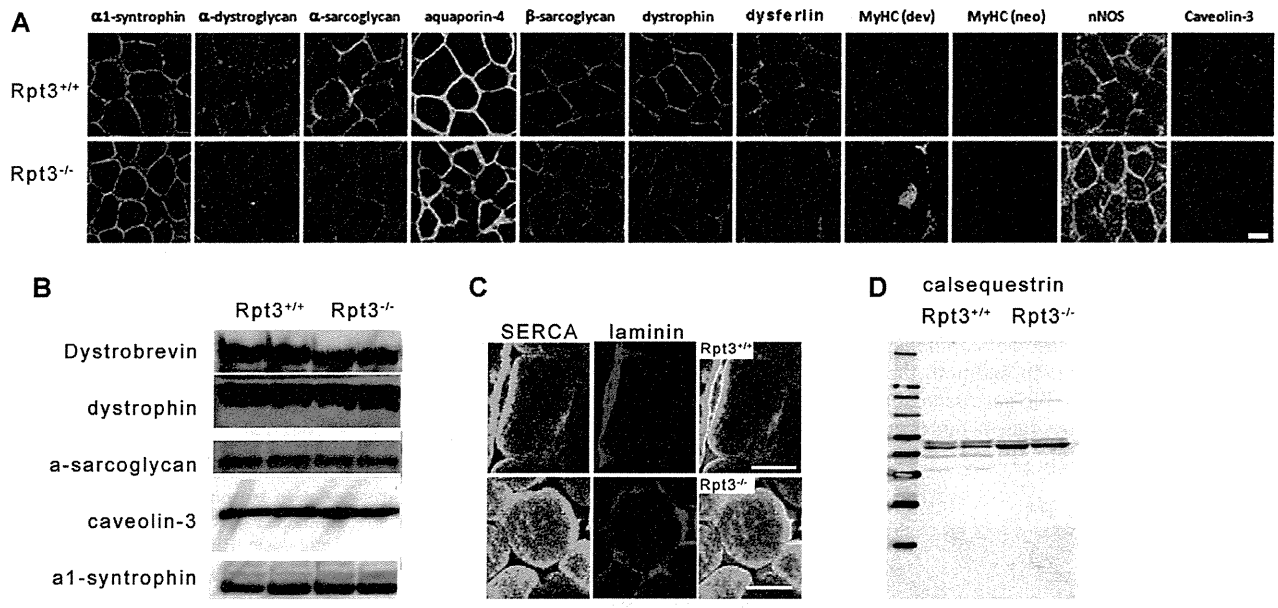


**Fig. 3. Immunohistochemistry and immunoblotting of the dystrophin glycoprotein complex and sarcoplasmic reticulum proteins in the gastrocnemius of Rpt3$^{-/-}$ and Rpt3$^{+/+}$ mice.** (A,B) Immunohistochemistry and immunoblotting of the components of the dystrophin glycoprotein complex in 6-week-old mice. No apparent differences were observed in α1-syntrophin, α-dystroglycan, α-sarcoglycan, aquaporin-4, β-sarcoglycan, dystrophin, dysferlin, neuronal nitric oxide synthetase or caveolin-3 levels. A small amount of developmental myosin heavy chain was observed in muscles from Rpt3$^{-/-}$ mice. Neonatal myosin heavy chain was not observed. Scale bar: 50 μm. (C,D) Immunohistochemistry and immunoblotting to detect the sarcoplasmic-reticulum-related proteins SERCA1 (C) and calsequestrin (D).

synthetase or caveolin-3 levels based on immunohistochemical examination (Fig. 3A). A small amount of developmental myosin heavy chain was observed in the gastrocnemius muscle tissue of Rpt3$^{-/-}$ mice (Fig. 3A), suggesting the presence of a regenerative process that most likely counteracts fast-twitch muscle fiber degeneration, which leads to an increased serum creatine kinase level (Fig. 1K). The fluorescence corresponding to SERCA protein expression was higher in Rpt3$^{-/-}$ gastrocnemius muscle tissue compared with that of Rpt3$^{+/+}$ muscle tissue by immunohistochemical analysis (Fig. 3C). A higher level of calsequestrin in Rpt3$^{-/-}$ gastrocnemius muscle was demonstrated by immunoblotting analysis (Fig. 3D). The increase in these sarcoplasmic reticulum proteins corresponds to the morphological change in the sarcoplasmic reticulum (Fig. 2F–I).

### Altered proteolysis in Rpt3$^{-/-}$ mice

To investigate the effect of Rpt3 deletion on proteasomal activity in skeletal muscle tissue, a knockdown of Rpt3 by small interfering (si)RNA in C2C12 cultured myoblasts was performed. Proteasomal activity was markedly reduced in C2C12 cells after siRNA-mediated Rpt3 knockdown at 24, 48 and 72 h after transfection (Fig. 4A,B). In the immunoblotting analysis, the Rpt3 band was undetectable after siRNA treatment, indicating that the Rpt3 antibody correctly detected the Rpt3 protein (Fig. 4C).

Then, to investigate the effect of Rpt3 deletion *in vivo*, both chymotrypsin-like and trypsin-like proteasomal activities in the fast-twitch-dominant tibialis anterior muscles of 2-week-old mice were examined. The proteasomal activity in the muscle homogenate from Rpt3$^{-/-}$ mice was significantly lower compared with that from Rpt3$^{+/+}$ mice at 2 weeks of age (Fig. 4D). Proteasomal activity at 6 weeks of age, however, was higher in the Rpt3-deleted animals compared with Rpt3$^{+/+}$ mice (Fig. 4E). To examine whether the detected chymotrypsin-like and trypsin-like activities were proteasome-dependent, a highly specific proteasomal inhibitor, AdaAhx$_3$L$_3$VS (30 μM), was added to the muscle homogenates. The proteasome-specific inhibitor significantly reduced both the chymotrypsin-like and trypsin-like proteasome activities of tibialis anterior muscles from 6-week-old Rpt3$^{-/-}$ and Rpt3$^{+/+}$ mice (Fig. 4E). Therefore, the increased proteasomal activity in Rpt3$^{-/-}$ mice might not be due to the recovery or acquisition of Rpt3 because the Rpt3 protein was still markedly reduced at 6 weeks of age in Rpt3$^{-/-}$ mice (Fig. 4F). Indeed, corresponding to the enhanced chymotrypsin-like and trypsin-like proteolytic activity, the transcription of proteasomal components in the proteolytic subunits of the 20S catalytic core, including PSMB5 with chymotrypsin-like activity and PSMB7 with trypsin-like activity, was markedly activated in the tibialis anterior muscle homogenate (supplementary material Fig. S2).

A morphological comparison of tibialis anterior muscle tissue from 2-week-old and 6-week-old Rpt3$^{+/+}$ and Rpt3$^{-/-}$ mice (Fig. 4G) demonstrated a clearly increased number of irregularly shaped abnormal muscle fibers in 6-week-old mice that were characterized by swelling and dislocated and enlarged nuclei. The interstitial spaces were extended, and the number of infiltrating cells was increased.

An examination of the protein components of the proteasome other than Rpt3 in tibialis anterior muscle tissue revealed increased expression of Rpt2 (also known as PSMC1) in 6-week-old Rpt3$^{-/-}$ mice (Fig. 4H). No significant difference in the protein level of Rpt6 (also known as PSMC5), the binding partner of Rpt3, was identified in Rpt3$^{-/-}$ mice compared with Rpt3$^{+/+}$ mice (Fig. 4H). In addition, no significant differences in the protein levels of Rpt5, PA28α (also known as PSMC3, PSME1, respectively) or 20S proteasome proteins were noted between Rpt3$^{+/+}$ and Rpt3$^{-/-}$ mice (Fig. 4H).





Journal of Cell Science

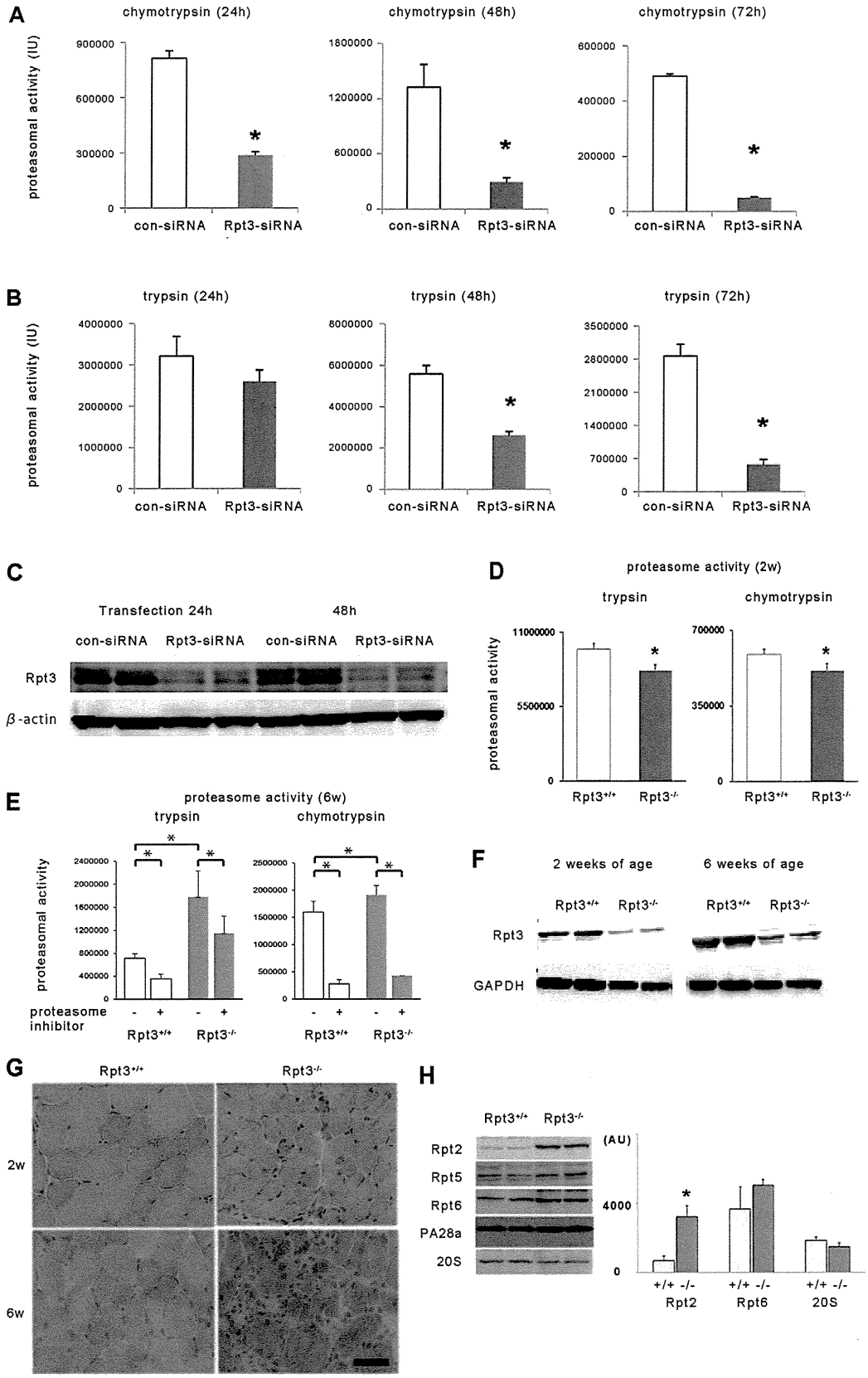


**Fig. 4. The effect of Rpt3 knockdown and Rpt3 deletion on proteasomal activity *in vitro* and *in vivo*.** The chymotrypsin-like (A) and trypsin-like (B) activities of control (con-siRNA)- and Rpt3-siRNA-transfected C2C12 cells were assessed. Proteasomal activity was significantly suppressed in Rpt3-siRNA-transfected cells. Proteasomal activity at 24, 48 and 72 h after transfection is shown. IU, international units. (C) Rpt3 protein expression was suppressed in Rpt3-siRNA-transfected C2C12 cells. (D) Proteasomal activity (trypsin-like and chymotrypsin-like activity) in the tibialis anterior muscles of 2-week-old $Rpt3^{-/-}$ and $Rpt3^{+/+}$ mice ($n$=5). (E) Proteasomal activity (trypsin-like and chymotrypsin-like activity) in the tibialis anterior muscles of 6-week-old $Rpt3^{-/-}$ and $Rpt3^{+/+}$ mice ($n$=6). Trypsin-like and chymotrypsin-like activity were increased in $Rpt3^{-/-}$ mice compared with $Rpt3^{+/+}$ mice. The highly specific proteasomal inhibitor $AdaAhx_3L_3VS$ (30 μM) significantly suppressed chymotrypsin-like activity by >70%, and trypsin-like activity by >30% from tibialis anterior muscle homogenate of both 6-week-old $Rpt3^{-/-}$ and $Rpt3^{+/+}$ mice. (F) Immunoblotting of Rpt3 protein using homogenates of tibialis anterior muscles from 2- and 6-week-old mice. (G) HE staining of tibialis anterior muscles from 2- and 6-week-old mice. Scale bar: 50 μm. (H) Changes in the components of the proteasomal complex of the tibialis anterior muscles. Rpt2 is significantly increased in $Rpt3^{-/-}$ mice compared with its expression in $Rpt3^{+/+}$ mice. White bars, $Rpt3^{+/+}$; gray bars, $Rpt3^{-/-}$. AU, arbitrary units. All quantitative data show the mean+s.e.m.; *$P$<0.05 (Student's $t$-test).





Journal of Cell Science

### The transcriptional and protein levels of ubiquitin proteasomal components and the upstream pathway in Rpt3$^{-/-}$ mice

Because the activity of the ubiquitin proteasomal pathway depends upon an upstream transcriptional program that requires the activation of a subset of atrophy-related genes, or atrogenes (Lecker et al., 2004), the expression of atrogenes involved in the ubiquitin–proteasomal pathway in the fast-twitch-dominant gastrocnemius muscle of Rpt3$^{-/-}$ mice was examined. Indeed, the protein and transcriptional levels of two atrophy-related ubiquitin E3 ligases, MuRF1 and atrogin-1, were markedly increased in Rpt3$^{-/-}$ mouse gastrocnemius muscle compared with that of Rpt3$^{+/+}$ mice (Fig. 5A,B). The levels of ubiquitin and polyubiquitylated protein at the Lys48 residue were also markedly increased (Fig. 5C). An immunohistochemical examination also demonstrated a marked increase or accumulation of polyubiquitylated proteins in the fast-twitch muscle fibers of the gastrocnemius muscle from Rpt3$^{-/-}$ mice (Fig. 5D).

To obtain an overall view of the gene expression profiles in Rpt3$^{-/-}$ skeletal muscle, microarray and real-time PCR analyses of gastrocnemius muscle tissue were performed (Fig. 5E,F; primers are listed in supplementary material Table S1). Proteasome-related genes were upregulated in Rpt3$^{-/-}$ mice; a summary of the top ten networks identified by Ingenuity pathway analysis of the microarray data revealed that 'connective tissue proliferation', 'cellular development' and 'protein synthesis' were all affected in Rpt3$^{-/-}$ mice (supplementary material Table S2). The microarray data are available online (GEO; http://www.ncbi.nlm.nih.gov/geo/) under the accession number GSE34896. A pathway analysis using DAVID online software provided by the National Institute of Allergy and Infectious Diseases (NIAID), NIH (http://david.abcc.ncifcrf.gov/home.jsp) was performed. A KEGG pathway analysis using the list of genes that were differentially expressed over 1.5-fold compared with their expression in Rpt3$^{+/+}$ mice is shown in supplementary material Table S3. Proteasome- and lysosome-related genes were significantly upregulated, as was the MAPK pathway in Rpt3$^{-/-}$ mice (supplementary material Table S3). The protein level of phosphorylated p38 was increased in the gastrocnemius muscle of the Rpt3$^{-/-}$ mice (Fig. 7A).

The autophagy pathway is another important mechanism that is responsible for protein degradation and processing within cells. The protein p62 (also known as SQSTM1) has a role in the aggregation of intracellular ubiquitin-related protein (Komatsu et al., 2007). LC3 (also known as MAP1LC3A and MAP1LC3B) is a post-translational modifier that is essential for autophagosome formation. The protein and transcriptional levels of p62 were markedly increased in Rpt3$^{-/-}$ mouse gastrocnemius muscle compared with the same muscle from Rpt3$^{+/+}$ mice (Fig. 6A,B). There was also an increase in LC3II and a marked decrease in the LC3II:LC3I ratio in Rpt3$^{-/-}$ mice (Fig. 6A). Immunohistochemical analyses detected a marked increase in the amount of p62 and LC3 in the myofibers of Rpt3$^{-/-}$ mutant animals (Fig. 6C,D).

The influence of Rpt3 deficiency on autophagy flux was examined in cultured C2C12 cells. The administration of the lysosome inhibitor chloroquine to C2C12 cells with or without Rpt3 siRNA resulted in an increase in LC3II protein (Fig. 6E,F), but the increase was attenuated in the Rpt3-knockdown C2C12 cells.

The levels of phosphorylated p38, phosphorylated Foxo3a, Foxo3a, p50 (also known as NFKB1) and myostatin were increased in the gastrocnemius muscle of Rpt3$^{-/-}$ mice (Fig. 7A,B). Although the protein level of Foxo3a was significantly higher in Rpt3$^{-/-}$ mice, no difference in the ratio of Foxo3a to its phosphorylated form was detected between Rpt3$^{-/-}$ and Rpt3$^{+/+}$ mice. The protein levels of p70S6K1 and the ratios of phosphorylated S6 (also known as RPS6), 4EBP1 and Akt were similar in gastrocnemius muscles from both Rpt3$^{+/+}$ and Rpt3$^{-/-}$ mice (Fig. 7A,B). Additionally, the total amount of 4EBP1 and phosphorylated 4EBP1 was increased. Therefore, the downregulation of protein synthesis did not likely contribute to muscle atrophy or the degeneration of Rpt3$^{-/-}$ muscle in this study.

Several diseases are characterized by abnormal protein aggregates in myofibers. The expression of TDP-43 and fused in sarcoma/translocated in liposarcoma (FUS/TLS) has been observed in muscle biopsy samples from patients with sporadic inclusion body myositis (sIBM) (Weihl and Pestronk, 2010; Yamashita et al., 2013). The amounts of these proteins differed between Rpt3$^{+/+}$ and Rpt3$^{-/-}$ mice, particularly in the insoluble fraction, when evaluated by immunoblotting (Fig. 7C). Immunohistochemical examination revealed enhanced staining of TDP-43, FUS/TLS and VCP in the myonuclei of gastrocnemius muscle from Rpt3$^{-/-}$ mice (Fig. 7D).

## DISCUSSION

In this study, we report that the fast-twitch muscle-specific deletion of a crucial proteasomal gene, *Rpt3*, resulted in profound muscle growth defects and a decrease in force production in mice with the accumulation of abnormal proteins. To the best of our knowledge, our study is the first to examine the role of the proteasomal system in mammalian skeletal muscle using a loss-of-function strategy. Contrary to our hypothesis and previous studies using proteasome inhibitors on dystrophic mice or myostatin-defective mice, in which muscle hypertrophy was demonstrated (McPherron et al., 1999), the specific deletion of the proteasome component Rpt3 led to a significant loss of muscle mass with premature death and significantly reduced physical activity.

To generate a skeletal-muscle-specific Rpt3 conditional knockout, we used Cre under the control of the Mlc1f promoter, with which we could delete Rpt3 only in fast-twitch muscle fibers. We first used α1 skeletal muscle actin promoter (ACTA1)-Cre transgenic mice so that Cre would be expressed without fiber-type specificity; however, this deletion resulted in embryonic lethality. The skeletal muscle creatine kinase (MCK)-Cre transgenic, which is often used to establish muscle-specific loss of function, was also a candidate, but we did not use this line because the MCK-Cre transgenic is known also to induce Cre in cardiac muscle tissue. Therefore, although we failed to demonstrate the histological distribution of Rpt3 in muscle tissue, most likely owing to the non-specific binding of the Rpt3 polyclonal antibody, the expression of Rpt3 in slow-twitch fibers might not have been affected.

In this study, because there was no difference in the size of slow-twitch fibers between Rpt3$^{+/+}$ and Rpt3$^{-/-}$ mice and because the proportion of slow-twitch muscle was increased in the gastrocnemius muscle of Rpt3$^{-/-}$ mice at older age, we assume that there was a selective reduction of fast-twitch fibers in the gastrocnemius muscle. The premature death observed in Rpt3$^{-/-}$ mice might be a consequence of impaired fast-twitch fibers. The movement of Rpt3$^{-/-}$ mice was slow with a significantly reduced step pace. The impaired movement might



Journal of Cell Science

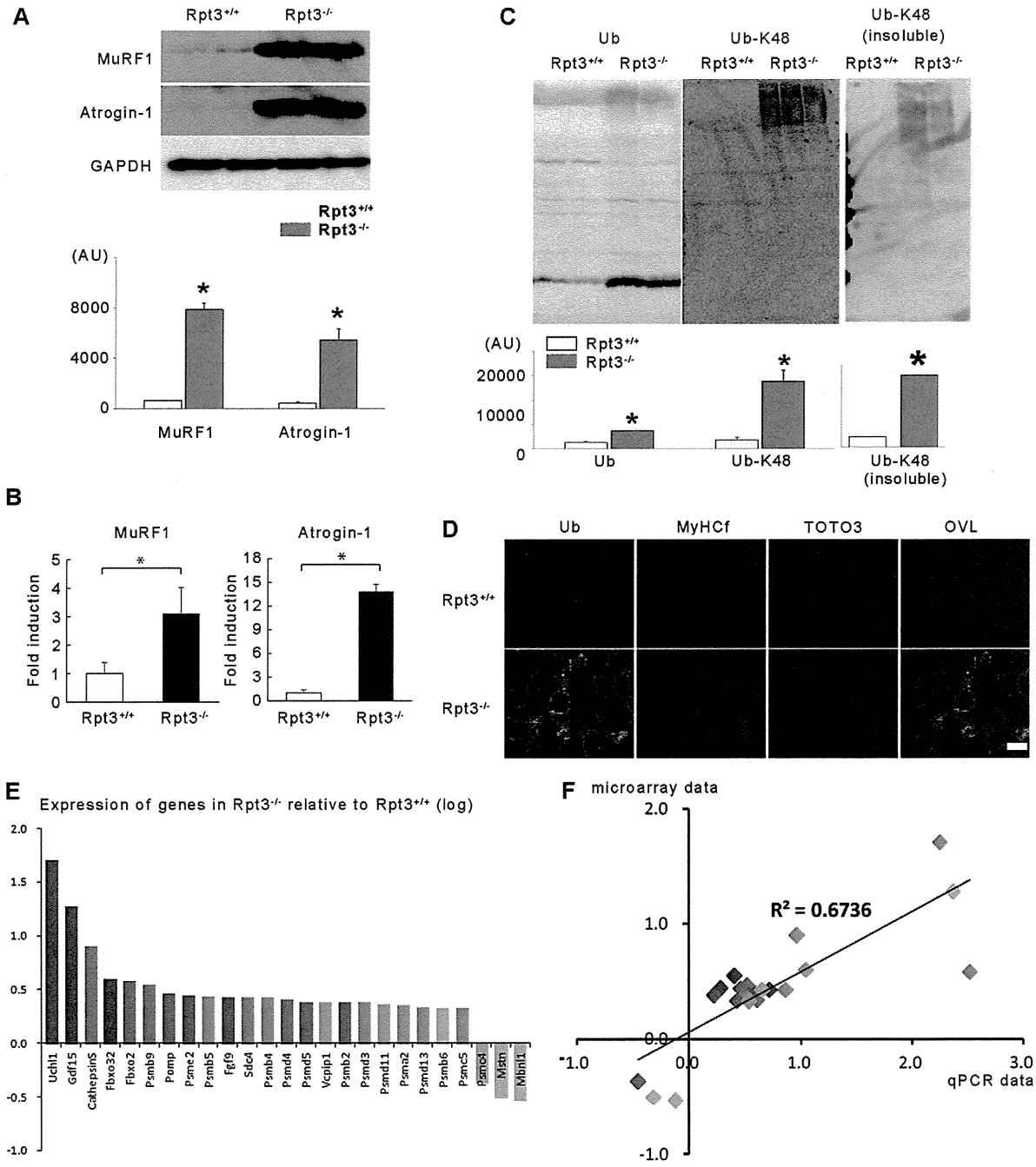


**Fig. 5. The ubiquitin–proteasome pathway is dysregulated in the gastrocnemius muscles of Rpt3$^{-/-}$ mice.** (A) Protein levels of the muscle-specific ubiquitin-E3-ligases MuRF1 and atrogin-1 were higher in Rpt3$^{-/-}$ mice than in Rpt3$^{+/+}$ mice at the age of 6 weeks. Quantitative data are also presented ($n$=3). AU, arbitrary units. (B) Upregulation of the crucial atrophy-related and muscle-specific genes in Rpt3$^{-/-}$ mice at the age of 6 weeks. RNA was extracted from the gastrocnemius muscles, and quantitative PCR analysis was performed in triplicate using specific primers (supplementary material Table S1). Data were normalized to the GAPDH content and expressed as the fold increase over the expression levels in Rpt3$^{+/+}$ mice ($n$=5). (C) The levels of ubiquitin (Ub) and high-molecular-mass ubiquitylated proteins were increased in Rpt3$^{-/-}$ mice. Protein polyubiquitylated at the Lys48 residue (detected using an anti-Ub-K48 antibody) was also increased in Rpt3$^{-/-}$ mice. Quantitative data are also presented ($n$=3). Quantitative data in A–C show the mean+s.e.m.; *$P$<0.05 (Student's $t$-test). (D) Immunohistochemical detection of ubiquitin and MyHCf revealed the accumulation of ubiquitylated proteins, particularly in fast-twitch muscle fibers. TOTO3, nuclei; OVL, overlay. Scale bar: 50 μm. (E) Upregulation of crucial proteasome-related genes in the skeletal muscles of adult Rpt3$^{-/-}$ mice. RNA was extracted from the gastrocnemius muscles. The $y$-axis represents the quantitative values of gene expression in Rpt3$^{-/-}$ mice relative to Rpt3$^{+/+}$ mice, which were transformed to $\log_{10}$ values. The value '0' indicates equal gene expression between Rpt3$^{-/-}$ and Rpt3$^{+/+}$ mice. Of the several proteasome-related genes that were measured, the expression of PSMC4 (Rpt3) was inhibited in Rpt3$^{-/-}$ mice compared with that of Rpt3$^{+/+}$ mice. Quantitative PCR analysis was performed in triplicate using specific primers (supplementary material Table S1). (F) Relative expression levels, normalized to β-actin, were well correlated between the microarray data and the quantitative PCR analysis ($R^2$=0.6736).





Journal of Cell Science

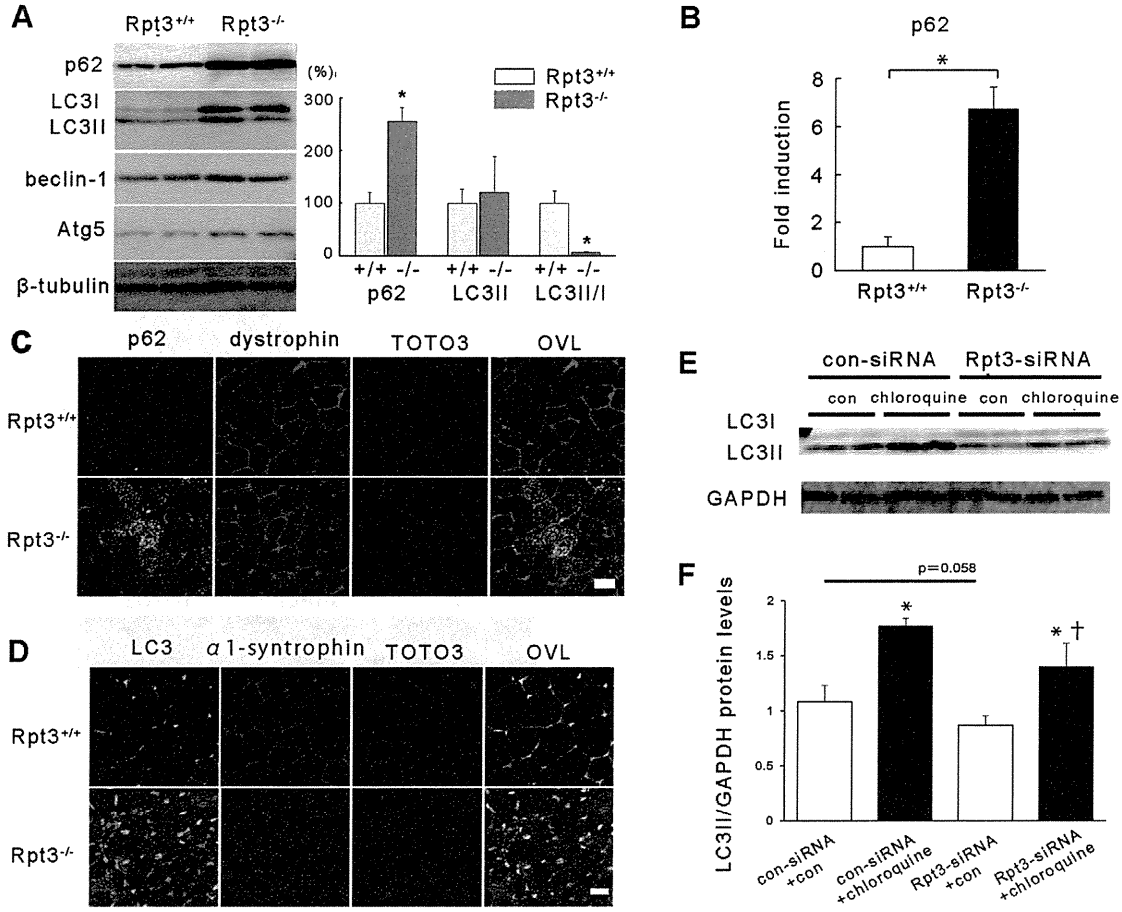


**Fig. 6. Autophagy is reduced in the gastrocnemius muscles of Rpt3$^{-/-}$ mice.** (A) Immunoblotting revealed increased levels of p62, LC3, beclin-1 and Atg5 proteins in Rpt3$^{-/-}$ mice at the age of 6 weeks. Quantitative data are also presented ($n$=3). Note that p62 was increased and the LC3II:LC3I ratio was decreased in Rpt3$^{-/-}$ mice. (B) Upregulation of p62 mRNA in Rpt3$^{-/-}$ mice at the age of 6 weeks. RNA was extracted from the gastrocnemius muscles, and quantitative PCR analysis was performed in triplicate using specific primers (supplementary material Table S1). Data were normalized to the GAPDH content and expressed as the fold increase over the level of expression in Rpt3$^{+/+}$ mice ($n$=5). (C) Immunohistochemical examination revealed p62-positive myofibers in Rpt3$^{-/-}$ mice at the age of 6 weeks. Scale bar: 50 μm. (D) Immunohistochemical examination revealed LC3-positive myofibers in Rpt3$^{-/-}$ mice at the age of 6 weeks. TOTO3, nuclei; OVL, overlay. Scale bar: 50 μm. (E) Autophagy flux was investigated using C2C12 cells. Representative immunoblotting showing autophagy flux assay with reduced LC3II levels following Rpt3 knockdown under chloroquine inhibition ($n$=4/treatment). con, control. (F) The protein level of LC3II was significantly different between vehicle- and chloroquine-treated samples (*$P$<0.05). The protein level of LC3II was significantly different between samples treated with both Rpt3 siRNA and chloroquine and those treated with control siRNA and chloroquine ($^{\dagger}P$<0.05). The protein level of LC3II was not significantly different between samples treated with control siRNA without chloroquine those treated with Rpt3 siRNA without chloroquine ($P$=0.058). Quantitative data in A,B,F show the mean+s.e.m.; *$P$<0.05 (Student's $t$-test).

have limited their access to food, but the precise cause of premature death remains unknown. However, not all fast-twitch fibers were lost because the tibialis anterior muscle, of which >99% is fast-twitch fibers (Augusto et al., 2004), maintained fast-twitch fibers even at 6 weeks of age.

Proteasomal activity was significantly reduced in the whole-muscle preparation at 2 weeks of age as measured both by chymotrypsin-like and trypsin-like activity in the Rpt3$^{-/-}$ mice. The fact that Rpt3 knockdown in C2C12 myoblasts led to a >80% reduction in proteasomal activity suggests that at the single fast-twitch fiber level, proteasomal activity was largely abrogated in Rpt3$^{-/-}$ mice. The reason that the reduction in proteasomal activity in tibialis anterior muscle remained at only ~20% *in vivo* at the age of 2 weeks might be due to the excision efficiency of the Mlc1f-promoter-driven Cre, which is ~40–50% (Bothe et al., 2000). Therefore, some myonuclei that were positive for *Rpt3* might have remained. Additionally, non-muscle cells, such as inflammatory cells, might have contributed to the proteasomal activity.

The results obtained in this study markedly contrasted with the results obtained in previous studies using the proteasome inhibitor MG-132, in which the administration of MG-132 significantly improved the dystrophic phenotype (Carmignac et al., 2011). MG-132 also improved the dystrophic phenotype in a model of dystrophin deficiency (Bonuccelli et al., 2003; Winder et al., 2011). The administration of MG-132 might have effects on all tissues and organs. Specifically, MG-132 is known to protect IκB, which inhibits NFκB, from proteasomal degradation in inflammatory cells. Thus, an attenuated inflammatory process might have favored mice with a dystrophin deficiency (Lee and Goldberg, 1998). This was one of our strong motivations to establish a skeletal muscle-specific deletion of the Rpt3





Journal of Cell Science

Journal of Cell Science (2014) 127, 5204–5217 doi:10.1242/jcs.150961

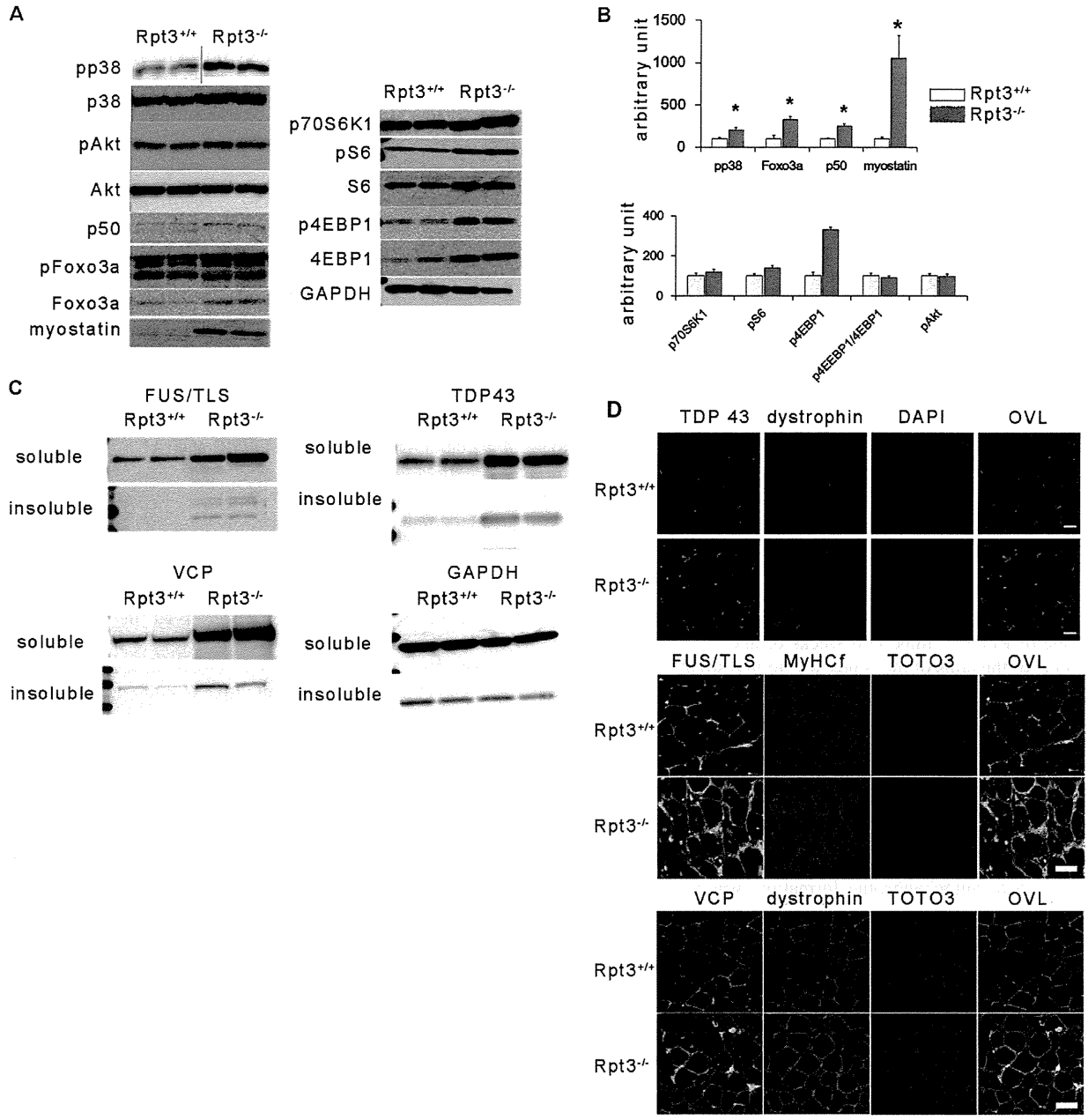


**Fig. 7. Catabolic pathways in the gastrocnemius muscles of Rpt3$^{-/-}$ mice.** (A) Immunoblotting analysis for the detection of muscle atrophy-related signaling pathway components. (B) Quantification of the data from A. The amount of phosphorylated p38 (pp38) was also increased in Rpt3$^{-/-}$ mice. No apparent differences were observed in the levels of Akt and phosphorylated (p)Akt. Foxo3a, p50, and myostatin were increased. Phosphorylated (p)Foxo3a, p70S6K1, phosphorylated (p)S6, S6, phosphorylated (p)4EBP1, 4EBP1 and GAPDH were also present. The ratios of phosphorylated S6:S6 and phosphorylated 4EBP1:4EBP1 were not altered, whereas the total amount of phosphorylated 4EBP1 was increased. Data show the mean+s.e.m.; *$P$<0.05 (Student's $t$-test). (C) Proteins related to RNA metabolism accumulated in myofibers. Expression of the FUS/TLS, VCP and TDP-43 proteins was increased in Rpt3$^{-/-}$ mice, especially in the insoluble fractions. (D) Immunohistochemistry of TDP-43, FUS/TLS and VCP revealed that the amount of these markers localizing within myonuclei in Rpt3$^{-/-}$ mice was increased. TOTO3, nuclei; OVL, overlay. Scale bars: 20 μm (upper panel), 50 μm (middle and lower panels).

component of the proteasome complex without affecting non-muscle cell types, such as inflammatory cells, in order to achieve a better understand the role of the ubiquitin–proteasome pathway in skeletal muscle cells.

Interestingly, although the proteasomal activity was significantly suppressed in Rpt3$^{-/-}$ fast-twitch dominant skeletal muscles at 2 weeks of age, a marked enhancement, rather than a mere recovery, in trypsin-like and chymotrypsin-like proteasomal activity was observed in the skeletal muscle at 6 weeks of age. Indeed, the transcription of the proteasomal components PSMB5 with chymotrypsin-like activity and PSMB7 with trypsin-like activity, which are proteolytic subunits of the 20S catalytic core, was markedly increased in Rpt3$^{-/-}$ mice at 6 weeks of age. Some possibilities might explain the apparent





Journal of Cell Science

enhancement in proteolytic activity, and these issues need to be further addressed. First, the involvement of proteolytic activity from a non-proteasomal source, such as lysosomes, is not likely because the proteolytic activity in the muscle homogenate of the tibialis anterior muscle was sensitive to a highly specific proteasome inhibitor. Second, because the tibialis anterior muscle is composed mostly of fast-twitch fibers and there was no fiber-type switching in Rpt3$^{-/-}$ mice, the possibility of the contribution of intact proteasomes from slow-twitch fibers should be almost negligible (supplementary material Fig. S1). One of the more plausible explanations for the increase in proteasomal proteolytic activity at an older age is the upregulation of the proteolysis pathways that counteract the reduced degradation of ubiquitylated proteins. An increased amount of the ubiquitin E3 ligases MuRF1 and atrogin-1 in Rpt3$^{-/-}$ gastrocnemius muscle might also have contributed to the accumulation of ubiquitylated proteins, but this result could also be a part of a counteraction against impaired protein degradation through proteasomes. Although no change was found in the ratio between Foxo3a and its phosphorylated form, the amount of Foxo3, which transcriptionally activates MuRF1 and atrogin-1 expression, was higher in Rpt3$^{-/-}$ compared with Rpt3$^{+/+}$ mice. The apparent myocellular effort of counter-regulation against impaired protein degradation, however, did not seem to be effective in the restoration of effective protein degradation because there was a remarkable accumulation of ubiquitylated proteins in the muscle tissue of Rpt3$^{-/-}$ mice at 6 weeks of age.

One of the aims of this study was to investigate the influence of autophagy activity when proteasomal function was impaired. In Rpt3$^{-/-}$ muscle tissue, the initial steps to transfer ubiquitylated proteins to the autophagy pathway seem to be enhanced. Ubiquitin-binding p62 was markedly increased by more than twofold in Rpt3$^{-/-}$ gastrocnemius muscle, and immunostaining of p62 was detected within Rpt3$^{-/-}$ muscle fibers. Beclin-1 and Atg-5 that are involved in isolation membrane formation were also increased in Rpt3$^{-/-}$ tissue. LC3I, which is involved in the initiation of autophagosome formation, was markedly increased in Rpt3$^{-/-}$ gastrocnemius muscle. To this extent, the autophagy pathway seems to be enhanced. Although the LC3I protein level was markedly increased in Rpt3$^{-/-}$ gastrocnemius muscle homogenate at 6 weeks of age, the conversion to LC3II (LC3II:LC3I) was significantly reduced. Therefore, the progression of autophagolysosomal formation seems to be impaired. An independent cellular study using cultured C2C12 myotubes revealed that Rpt3 knockdown resulted in the suppression of LC3 turnover, suggesting a contribution of the proteasomal proteolytic process in autophagy progression. Taken together, a cellular effort appears to compensate for impaired proteasomal proteolysis caused by the absence of Rpt3 in the proteasomal complex by delivering ubiquitylated proteins to the autophagy pathway, but autophagy seems to be impaired at autophagosome formation by an unknown but proteasomal-activity-dependent mechanism. The lack of increase in the number of autophagosomes as revealed by electron microscopy might correspond to this observation. Increased myostatin expression might also have contributed to the enhanced expression of autophagy proteins (Lee et al., 2011).

The increase in p62 and the formation of inclusion bodies observed in Rpt3$^{-/-}$ mice was previously reported as a pathophysiological condition induced by a deficiency in autophagy (Komatsu et al., 2007). In addition to muscle atrophy, we also observed a marked increase in proteins associated with myopathies and neurodegenerative diseases, such as VCP, TDP-43 and FUS/TLS, within the muscle fibers of Rpt3$^{-/-}$ mice. Indeed, VCP is a molecular adapter that binds to the ubiquitin of a ubiquitylated protein and autophagosome-specific proteins (Tresse et al., 2010). The concomitant increase in VCP and p62 seems to be reasonable. These proteins might be cooperating in transferring accumulated ubiquitylated proteins to the selective autophagy pathway. The accumulation of TDP-43 within the nuclei of Rpt3$^{-/-}$ myofibers is another interesting finding. TDP-43 is an RNA-binding protein suggested to be required for the maintenance of the autophagy pathway by stabilizing *Atg7* mRNA (Bose et al., 2011). A marked increase in TDP-43 might further support the compensatory activation of the selective autophagy pathway due to impaired proteasomal activity. The FUS/TLS protein also has RNA binding capability, has a transcriptional activation property (Fiesel and Kahle, 2011) and is enhanced in Rpt3$^{-/-}$ muscle myonuclei; however, the distinct role of this protein in the Rpt3$^{-/-}$ pathology is unknown. TDP-43, FUS/TLS and p62 are integral components of sIBM inclusions, with p62 immunoreactivity being particularly specific and strong, and these proteins can be used as disease markers for sIBM (Nogalska et al., 2009; Salajegheh et al., 2009). Our finding in this study suggests that the pathological mechanism might be similar to that of sIBM, although electron microscopic analysis of Rpt3$^{-/-}$ mice did not reveal myelin-like structures similar to those observed in patients with sIBM. Proteasomal activity in the muscles of patients with sIBM is reported as either activated or suppressed (Ferrer et al., 2005; Fratta et al., 2005); thus, multiple pathological mechanisms might be involved. Our findings might partly explain the pathology of sIBM with suppressed proteasomal activity.

Impaired autophagy is known to induce skeletal myofiber degeneration and muscle weakness (Masiero et al., 2009; Raben et al., 2008). Using the same Mlcf-Cre promoter, Masiero et al. generated fast-twitch muscle-specific *Atg7*-knockout mice to disrupt the autophagy pathway in skeletal muscle (Masiero et al., 2009). We found similar myopathic changes in the Rtp3$^{-/-}$ mice as in the Atg7$^{-/-}$ mice, but the extent of muscle wasting or failure in muscle development was apparently more severe in the Rpt3$^{-/-}$ mice. The body weight of Atg7$^{-/-}$ mice was reported to be slightly lower than that of the control mice, whereas Rpt3$^{-/-}$ mice exhibited a marked impairment in body weight growth mainly due to impaired muscle growth. We found not only weakness in muscle strength but also a serious gait disturbance due to muscle weakness. Premature death was observed in Rpt3$^{-/-}$ mice but not in Atg7$^{-/-}$ mice. Considering that the same fast-twitch muscle cells were affected in these conditional knockout mice, we conclude that the proteasomal pathway has a greater impact on maintaining the homeostasis of skeletal muscle tissue.

Referring to the fundamental role of autophagy, the autophagy process is promoted when cells are cultured under starved conditions without amino acids in the culture medium (Kuma and Mizushima, 2010). Our study suggests that both the ubiquitin proteasome and autophagy systems are required to maintain myocellular homeostasis and integrity. The protein and organelle degradation by both autophagy and ubiquitin proteasome systems might provide resources, such as oligopeptides and amino acids, for maintaining cellular integrity in skeletal muscle tissue (Bonaldo and Sandri, 2013). Therefore, the Rpt3 deficiency might have resulted in a far more serious condition that deprives the cells of two major paths of pooling resources for cellular



Journal of Cell Science

maintenance. We hypothesize that the skeletal muscle Rpt3 deficiency might have led to blocking the cellular 'recycling system' that is essential to the maintenance of skeletal muscle fibers, and this question needs to be further examined. In *Drosophila*, the progressive accumulation of protein aggregates is a characteristic of aging in skeletal muscle (Demontis and Perrimon, 2010). Using the conditional expression of a mutant proteasome β subunit in *Drosophila*, Haas et al. reported that the ubiquitin proteasome system is required for the acute maintenance of muscle and neuromuscular junction architecture (Haas et al., 2007). Taken together, these results suggest that basal, appropriately balanced proteasomal activity has a beneficial role in the control of muscle mass during muscle growth.

## MATERIALS AND METHODS

### Generation of muscle-specific Rpt3-knockout mice

Mice bearing a floxed Rpt3 allele (Tashiro et al., 2012) (Rpt3 f/f) were crossed with transgenic mice expressing Cre under the control of either a myosin light chain 1 fast promoter (MLC1f-Cre) (Bothe et al., 2000) or an α1 skeletal muscle actin promoter (ACTA1-Cre) (Miniou et al., 1999). Genomic DNA isolated from mice bearing the Cre allele or Rpt3-lox was subjected to standard PCR analysis. The animals were provided access to food and drinking water *ad libitum* and were euthanized by cervical dislocation under anesthesia. The tibialis anterior and gastrocnemius muscles were subsequently excised for analysis. All of the experimental protocols and procedures were approved by the Animal Committee of the Tohoku University School of Medicine Ethics Committee (animal 2011-234).

### Mouse tissue preparation

Body and wet muscle weights were determined. Tibialis anterior and gastrocnemius muscles were collected individually using standard dissection methods and cleared of excess fat, connective tissue and tendons, and subjected to further preparation and analyses. The origins of muscle samples either from tibialis anterior or gastrocnemius muscle is described in each figure legend. Some portions of the muscles were frozen in isopentane cooled with liquid nitrogen for histological and immunohistochemical analysis, and the other muscle portions were frozen directly in liquid nitrogen and stored at −80℃ for RNA isolation or protein extraction.

### Antibodies

Antibodies against the following proteins were obtained from Cell Signaling Technology: Akt, phosphorylated Akt (Ser473), phosphorylated p38, p38, ubiquitin, protein polyubiquitylated at the Lys48 residue (Ub-K48), Atg5, beclin-1, Hsp90, p70S6K1, phosphorylated S6 (Ser240/244), S6, phosphorylated 4EBP1 and 4EBP1. Antibodies against Rpt2, Rpt3, Rpt5, PA28α and 20S were purchased from Enzo. MuRF1 and atrogin-1 antibodies were purchased from ECM Biosciences. Calsequestrin antibodies were purchased from Abcam. Antibodies against fast, slow, developmental and neonatal myosin heavy chain and antibodies against dystrobrevin, dystrophin, α-dystroglycan, α-sarcoglycan and caveolin-3 were obtained from Novocastra. Serca and laminin antibodies were obtained from Sigma. We also used antibodies against GAPDH (Santa Cruz Biotechnology), LC3 (Novus Biological and nanoTools Antikörpertechnik), p62 (PROGEN Biotechnik), TDP-43 (Proteintech), FHL1 (Abcam), VCP (BD Biosciences), FUS/TLS (Bethyl Laboratories), α1-syntrophin (Thermo Fisher Scientific) and neuronal nitric oxide synthase (Invitrogen).

### Proteasome activity

Proteasome activity was assessed using Proteasome-Glo™ Assay kit (Promega) following the manufacturer's instruction. The trypsin-like and chymotrypsin-like activity assays were conducted using skeletal muscle homogenates in a total volume of 100 µl in opaque 96-well plates. For the assays, 120 µg of protein was added to assay buffer containing 20 mM Tris-HCl (pH 7.2), 0.1 mM EDTA, 5 mM ATP, 1 mM β-mercaptoethanol, 20% glycerol and 0.04% Nonidet P40. The individual proteasome reagents were added separately, and 30 min later, the luminescence was recorded as relative light units on a Varioskan luminometer (Thermo Scientific). Each sample was measured in triplicate.

In addition, to evaluate proteasome activity more precisely, dual measurements with or without the addition of 30 µM of the irreversible and highly specific proteasomal inhibitor adamantine-acetyl-(6-aminohexanoyl)$_3$-(leucinyl)$_3$-vinyl-(methyl)-sulfone (AdaAhx$_3$L$_3$VS, Calbiochem, catalog number 114802) were carried out (Kessler et al., 2001).

### Creatine kinase measurement

Blood (200 µl) was collected in Eppendorf tubes using cardiac puncture under deep anesthesia, and it was allowed to clot at room temperature prior to centrifugation and serum collection. Creatine kinase was measured using a standard spectrophotometric method according to the manufacturer's instructions. The data are expressed as units per liter.

### Functional tests

Forearm grip strength was assessed in 8-week-old mice using a grip strength meter (GPM-100, MelQuest) according to the manufacturer's instructions. An investigator blinded to the treatment conditions recorded three successful forelimb strength measurements ($n$=5) in the morning. The average grip strength measurement obtained each day was used for subsequent analysis. Motor endurance was measured using a round cage (RS-204-5, Kori-Seiki). The number of rotations per day was recorded, and the average number of rotations was calculated on three consecutive days ($n$=5).

### Step pace analysis

After conditioning runs, the plantar surface of the hind paws was impregnated with black printing paint and each mouse walked with office copier paper on the base. Four prints of each foot were recorded on the length of the paper used. The distance of the print length was measured as step pace (mm). The walking track test was performed at 6 weeks of age.

### Microarray analysis and real-time PCR

Total RNA was isolated using an RNeasy kit (Qiagen). The RNA was subjected to microarray analysis using a Codelink mouse whole-genome bioarray according to the manufacturer's instructions. We performed KEGG pathway analysis using the list of genes that were differentially expressed over 1.5 times from Rpt3$^{+/+}$ mice (supplementary material Table S3).

For real-time PCR, first-strand cDNA synthesis was performed using oligo-dT primers. The expression levels of selected genes were analyzed using the Bio-Rad CFX96 system according to the manufacturer's instructions and quantitative PCR analysis was performed in triplicate using specific primers (supplementary material Table S1).

### Immunohistochemistry

Cryosections of muscle tissue (10-µm thickness) were cut from the middle portion of the muscle belly to obtain the largest myofiber diameter, placed on poly-L-lysine-coated slides, air-dried, post-fixed in acetone at −20℃ and pre-incubated in phosphate-buffered saline (PBS) containing 5% goat serum and 1% bovine serum albumin (BSA) for 30 min at room temperature. The primary antibodies were applied overnight at 4℃. Following incubation with the appropriate secondary antibodies, the mounted sections were observed using an Olympus confocal microscope.

### Electron microscopy

The skeletal muscles were fixed using 4% paraformaldehyde and 2% glutaraldehyde for conventional electron microscopy. The samples were post-fixed with 1% $OsO_4$, embedded in Epon epoxy resin and sectioned.



Journal of Cell Science

### Immunoblotting analysis

The total skeletal muscle protein was extracted from the tibialis anterior muscles and gastrocnemius muscles for immunoblotting analysis. We described in the figure legends which muscles we used. We used the Bradford method to determine the total protein concentration. The protein fractions were then extracted with a reducing sample buffer containing 2.3% SDS, 70 mM Tris-HCl, 5% β-mercaptoethanol, and Complete Protease Inhibitor Cocktail (Roche). Proteins (30 μg per lane) were separated on a 10–20% gradient SDS-polyacrylamide gel and subsequently transferred to a polyvinylidene difluoride membrane (Millipore) at 240 mA for 1 h. The membrane was then incubated with primary antibody. Specific signals were detected using the enhanced chemiluminescence method (GE Healthcare), as described previously (Suzuki et al., 2007). Densitometry was performed using ImageJ software (National Institutes of Health). For the fractionation of soluble and insoluble proteins, a 6 M urea solution was used.

### C2C12 experiments

Mouse C2C12 myoblasts were cultured under standard conditions (37℃ under a humidified atmosphere containing 5% $CO_2$) in high-glucose DMEM supplemented with 10% fetal bovine serum and 100 μg/ml penicillin-streptomycin solution. The cells were transfected with 30 nM siRNA using Lipofectamine RNAiMAX (Invitrogen). To examine the proteasomal activity, C2C12 cells were harvested in the aforementioned assay buffer using a cell scraper at 24, 48 and 72 h after the transfection. After centrifugation (13,000 ***g*** for 15 min at 4℃), 100 μg of the cleared protein sample was incubated in the presence of 40 μM of fluorogenic substrate in reaction buffer. Autophagy flux was evaluated using the administration of 50 μM chloroquine (Sigma-Aldrich) as described previously (Mizushima et al., 2010).

### Statistical analysis

Significant differences were determined using either Student's unpaired *t*-test or the Mann–Whitney *U*-test. All data are expressed as the mean±s.e.m. Statistical significance was defined as $P<0.05$.

### Supplemental data

The microarray data have been deposited into the Gene Expression Omnibus (GEO; http://www.ncbi.nlm.nih.gov/geo/) under the accession number GSE34896. KEGG pathway analysis was performed using the list of genes differentially expressed over 1.5 times from $Rpt3^{+/+}$ mice (supplementary material Table S3).

### Acknowledgements

We thank Ayaka Sasaki, Naoko Shimakura, Toshiko Nakatani and Masumi Toyosawa (all of Tohoku University, Japan) for general technical support; Tetsuko Sueta and Tomomi Kibushi (both of Tohoku University, Japan) for animal handling; and Chika Tazawa and Hiroo Iwasa (both of Tohoku University, Japan) for electron microscopy. The MLC1f-Cre mice were kindly provided by Noboru Mizushima (Tohoku University, Japan) and Steven Burden (New York University, NY). We also thank Takafumi Hasegawa (Tohoku University, Japan), Shigeo Murata (Tokyo University, Japan), Ichizo Nishino and Shin'ichi Takeda (both of the National Center of Neurology and Psychiatry, Japan) for useful technics and discussions.

### Competing interests

The authors declare no competing interests.

### Author contributions

N.S. and M.Aoki conceived of the project; Y.K. and N.S. designed the overall experimental plan. Y.T., M.Y., M.Abe, K.S., H.I., M.U. and R.T. produced the animals. H.W. and M.K. performed staining. R.A performed animal experiments. M.T. and R.I. performed electron microscopy. Y.K. and R.N. performed cultures. N.S., Y.K., R.N. and M.Aoki wrote the manuscript.

### Funding

This work was supported by funding from 'Research on Measures for Intractable Diseases' and 'Research on Psychiatric and Neurological Diseases and Mental Health' from the Japanese Ministry of Health, Labor and Welfare; Grants-in-Aid for Scientific Research; an Intramural Research Grant for Neurological Psychiatric Disorders from the National Center of Neurology and Psychiatry; a Grant-in-Aid for Challenging Exploratory Research [grant numbers 22659167 and 24659421] from the Japanese Ministry of Education, Culture, Sports, Science and Technology; the Sasagawa Scientific Research Grant; the Takeda Science Foundation; and the Nakatomi Foundation. Deposited in PMC for immediate release.

### Supplementary material

Supplementary material available online at
http://jcs.biologists.org/lookup/suppl/doi:10.1242/jcs.150961/-/DC1

### Reference

**Augusto, V., Padovani, C. R. and Campos, G. E. R.** (2004). Skeletal muscle fiber types in C57BL6J mice. *Braz. J. Morphol. Sci.* **21**, 89-94.

**Bedford, L., Hay, D., Devoy, A., Paine, S., Powe, D. G., Seth, R., Gray, T., Topham, I., Fone, K., Rezvani, N. et al.** (2008). Depletion of 26S proteasomes in mouse brain neurons causes neurodegeneration and Lewy-like inclusions resembling human pale bodies. *J. Neurosci.* **28**, 8189-8198.

**Bonaldo, P. and Sandri, M.** (2013). Cellular and molecular mechanisms of muscle atrophy. *Dis. Model. Mech.* **6**, 25-39.

**Bonuccelli, G., Sotgia, F., Schubert, W., Park, D. S., Frank, P. G., Woodman, S. E., Insabato, L., Cammer, M., Minetti, C. and Lisanti, M. P.** (2003). Proteasome inhibitor (MG-132) treatment of mdx mice rescues the expression and membrane localization of dystrophin and dystrophin-associated proteins. *Am. J. Pathol.* **163**, 1663-1675.

**Bose, J. K., Huang, C. C. and Shen, C. K.** (2011). Regulation of autophagy by neuropathological protein TDP-43. *J. Biol. Chem.* **286**, 44441-44448.

**Bothe, G. W., Haspel, J. A., Smith, C. L., Wiener, H. H. and Burden, S. J.** (2000). Selective expression of Cre recombinase in skeletal muscle fibers. *Genesis* **26**, 165-166.

**Braun, T. and Gautel, M.** (2011). Transcriptional mechanisms regulating skeletal muscle differentiation, growth and homeostasis. *Nat. Rev. Mol. Cell Biol.* **12**, 349-361.

**Cai, D., Frantz, J. D., Tawa, N. E., Jr, Melendez, P. A., Oh, B. C., Lidov, H. G., Hasselgren, P. O., Frontera, W. R., Lee, J., Glass, D. J. et al.** (2004). IKKbeta/NF-kappaB activation causes severe muscle wasting in mice. *Cell* **119**, 285-298.

**Carmignac, V., Quéré, R. and Durbeej, M.** (2011). Proteasome inhibition improves the muscle of laminin α2 chain-deficient mice. *Hum. Mol. Genet.* **20**, 541-552.

**Demontis, F. and Perrimon, N.** (2010). FOXO/4E-BP signaling in Drosophila muscles regulates organism-wide proteostasis during aging. *Cell* **143**, 813-825.

**Ding, W. X., Ni, H. M., Gao, W., Yoshimori, T., Stolz, D. B., Ron, D. and Yin, X. M.** (2007). Linking of autophagy to ubiquitin-proteasome system is important for the regulation of endoplasmic reticulum stress and cell viability. *Am. J. Pathol.* **171**, 513-524.

**Ferrer, I., Carmona, M., Blanco, R., Moreno, D., Torrejón-Escribano, B. and Olivé, M.** (2005). Involvement of clusterin and the aggresome in abnormal protein deposits in myofibrillar myopathies and inclusion body myositis. *Brain Pathol.* **15**, 101-108.

**Fiesel, F. C. and Kahle, P. J.** (2011). TDP-43 and FUS/TLS: cellular functions and implications for neurodegeneration. *FEBS J.* **278**, 3550-3568.

**Fratta, P., Engel, W. K., McFerrin, J., Davies, K. J., Lin, S. W. and Askanas, V.** (2005). Proteasome inhibition and aggresome formation in sporadic inclusion-body myositis and in amyloid-beta precursor protein-overexpressing cultured human muscle fibers. *Am. J. Pathol.* **167**, 517-526.

**Glass, D. J.** (2010). Signaling pathways perturbing muscle mass. *Curr. Opin. Clin. Nutr. Metab. Care* **13**, 225-229.

**Grumati, P., Coletto, L., Sabatelli, P., Cescon, M., Angelin, A., Bertaggia, E., Blaauw, B., Urciuolo, A., Tiepolo, T., Merlini, L. et al.** (2010). Autophagy is defective in collagen VI muscular dystrophies, and its reactivation rescues myofiber degeneration. *Nat. Med.* **16**, 1313-1320.

**Haas, K. F., Woodruff, E., 3rd and Broadie, K.** (2007). Proteasome function is required to maintain muscle cellular architecture. *Biol. Cell* **99**, 615-626.

**Jagoe, R. T. and Goldberg, A. L.** (2001). What do we really know about the ubiquitin-proteasome pathway in muscle atrophy? *Curr. Opin. Clin. Nutr. Metab. Care* **4**, 183-190.

**Kaneko, T., Hamazaki, J., Iemura, S., Sasaki, K., Furuyama, K., Natsume, T., Tanaka, K. and Murata, S.** (2009). Assembly pathway of the Mammalian proteasome base subcomplex is mediated by multiple specific chaperones. *Cell* **137**, 914-925.

**Kessler, B. M., Tortorella, D., Altun, M., Kisselev, A. F., Fiebiger, E., Hekking, B. G., Ploegh, H. L. and Overkleeft, H. S.** (2001). Extended peptide-based inhibitors efficiently target the proteasome and reveal overlapping specificities of the catalytic beta-subunits. *Chem. Biol.* **8**, 913-929.

**Komatsu, M., Waguri, S., Koike, M., Sou, Y. S., Ueno, T., Hara, T., Mizushima, N., Iwata, J., Ezaki, J., Murata, S. et al.** (2007). Homeostatic levels of p62 control cytoplasmic inclusion body formation in autophagy-deficient mice. *Cell* **131**, 1149-1163.

**Kuma, A. and Mizushima, N.** (2010). Physiological role of autophagy as an intracellular recycling system: with an emphasis on nutrient metabolism. *Semin. Cell Dev. Biol.* **21**, 683-690.

**Lecker, S. H., Jagoe, R. T., Gilbert, A., Gomes, M., Baracos, V., Bailey, J., Price, S. R., Mitch, W. E. and Goldberg, A. L.** (2004). Multiple types of skeletal muscle atrophy involve a common program of changes in gene expression. *FASEB J.* **18**, 39-51.

**Lee, D. H. and Goldberg, A. L.** (1998). Proteasome inhibitors: valuable new tools for cell biologists. *Trends Cell Biol.* **8**, 397-403.

**Lee, J. Y., Hopkinson, N. S. and Kemp, P. R.** (2011). Myostatin induces autophagy in skeletal muscle in vitro. *Biochem. Biophys. Res. Commun.* **415**, 632-636.

**Li, H., Chen, Q., Liu, F., Zhang, X., Li, W., Liu, S., Zhao, Y., Gong, Y. and Yan, C.** (2013). Unfolded protein response and activated degradative pathways regulation in GNE myopathy. *PLoS ONE* **8**, e58116.

**Lyons, G. E., Ontell, M., Cox, R., Sassoon, D. and Buckingham, M.** (1990). The expression of myosin genes in developing skeletal muscle in the mouse embryo. *J. Cell Biol.* **111**, 1465-1476.

**Marx, F. P., Soehn, A. S., Berg, D., Melle, C., Schiesling, C., Lang, M., Kautzmann, S., Strauss, K. M., Franck, T., Engelender, S. et al.** (2007). The proteasomal subunit S6 ATPase is a novel synphilin-1 interacting protein—implications for Parkinson's disease. *FASEB J.* **21**, 1759-1767.

**Masiero, E., Agatea, L., Mammucari, C., Blaauw, B., Loro, E., Komatsu, M., Metzger, D., Reggiani, C., Schiaffino, S. and Sandri, M.** (2009). Autophagy is required to maintain muscle mass. *Cell Metab.* **10**, 507-515.

**McPherron, A. C., Lawler, A. M. and Lee, S. J.** (1999). Regulation of anterior/posterior patterning of the axial skeleton by growth/differentiation factor 11. *Nat. Genet.* **22**, 260-264.

**Miniou, P., Tiziano, D., Frugier, T., Roblot, N., Le Meur, M. and Melki, J.** (1999). Gene targeting restricted to mouse striated muscle lineage. *Nucleic Acids Res.* **27**, e27-e30.

**Mizushima, N., Yoshimori, T. and Levine, B.** (2010). Methods in mammalian autophagy research. *Cell* **140**, 313-326.

**Mourkioti, F., Slonimsky, E., Huth, M., Berno, V. and Rosenthal, N.** (2008). Analysis of CRE-mediated recombination driven by myosin light chain 1/3 regulatory elements in embryonic and adult skeletal muscle: a tool to study fiber specification. *Genesis* **46**, 424-430.

**Nishino, I., Fu, J., Tanji, K., Yamada, T., Shimojo, S., Koori, T., Mora, M., Riggs, J. E., Oh, S. J., Koga, Y. et al.** (2000). Primary LAMP-2 deficiency causes X-linked vacuolar cardiomyopathy and myopathy (Danon disease). *Nature* **406**, 906-910.

**Nogalska, A., Terracciano, C., D'Agostino, C., King Engel, W. and Askanas, V.** (2009). p62/SQSTM1 is overexpressed and prominently accumulated in inclusions of sporadic inclusion-body myositis muscle fibers, and can help differentiating it from polymyositis and dermatomyositis. *Acta Neuropathol.* **118**, 407-413.

**Raben, N., Hill, V., Shea, L., Takikita, S., Baum, R., Mizushima, N., Ralston, E. and Plotz, P.** (2008). Suppression of autophagy in skeletal muscle uncovers the accumulation of ubiquitinated proteins and their potential role in muscle damage in Pompe disease. *Hum. Mol. Genet.* **17**, 3897-3908.

**Ramachandran, N., Munteanu, I., Wang, P., Ruggieri, A., Rilstone, J. J., Israelian, N., Naranian, T., Paroutis, P., Guo, R., Ren, Z. P. et al.** (2013). VMA21 deficiency prevents vacuolar ATPase assembly and causes autophagic vacuolar myopathy. *Acta Neuropathol.* **125**, 439-457.

**Sakao, Y., Kawai, T., Takeuchi, O., Copeland, N. G., Gilbert, D. J., Jenkins, N. A., Takeda, K. and Akira, S.** (2000). Mouse proteasomal ATPases Psmc3 and Psmc4: genomic organization and gene targeting. *Genomics* **67**, 1-7.

**Salajegheh, M., Pinkus, J. L., Taylor, J. P., Amato, A. A., Nazareno, R., Baloh, R. H. and Greenberg, S. A.** (2009). Sarcoplasmic redistribution of nuclear TDP-43 in inclusion body myositis. *Muscle Nerve* **40**, 19-31.

**Salminen, A. and Kaarniranta, K.** (2009). Regulation of the aging process by autophagy. *Trends Mol. Med.* **15**, 217-224.

**Sandri, M., Sandri, C., Gilbert, A., Skurk, C., Calabria, E., Picard, A., Walsh, K., Schiaffino, S., Lecker, S. H. and Goldberg, A. L.** (2004). Foxo transcription factors induce the atrophy-related ubiquitin ligase atrogin-1 and cause skeletal muscle atrophy. *Cell* **117**, 399-412.

**Stitt, T. N., Drujan, D., Clarke, B. A., Panaro, F., Timofeyva, Y., Kline, W. O., Gonzalez, M., Yancopoulos, G. D. and Glass, D. J.** (2004). The IGF-1/PI3K/Akt pathway prevents expression of muscle atrophy-induced ubiquitin ligases by inhibiting FOXO transcription factors. *Mol. Cell* **14**, 395-403.

**Suzuki, N., Motohashi, N., Uezumi, A., Fukada, S., Yoshimura, T., Itoyama, Y., Aoki, M., Miyagoe-Suzuki, Y. and Takeda, S.** (2007). NO production results in suspension-induced muscle atrophy through dislocation of neuronal NOS. *J. Clin. Invest.* **117**, 2468-2476.

**Tashiro, Y., Urushitani, M., Inoue, H., Koike, M., Uchiyama, Y., Komatsu, M., Tanaka, K., Yamazaki, M., Abe, M., Misawa, H. et al.** (2012). Motor neuron-specific disruption of proteasomes, but not autophagy, replicates amyotrophic lateral sclerosis. *J. Biol. Chem.* **287**, 42984-42994.

**Todde, V., Veenhuis, M. and van der Klei, I. J.** (2009). Autophagy: principles and significance in health and disease. *Biochim. Biophys. Acta* **1792**, 3-13.

**Tresse, E., Salomons, F. A., Vesa, J., Bott, L. C., Kimonis, V., Yao, T. P., Dantuma, N. P. and Taylor, J. P.** (2010). VCP/p97 is essential for maturation of ubiquitin-containing autophagosomes and this function is impaired by mutations that cause IBMPFD. *Autophagy* **6**, 217-227.

**van Eersel, J., Ke, Y. D., Gladbach, A., Bi, M., Götz, J., Kril, J. J. and Ittner, L. M.** (2011). Cytoplasmic accumulation and aggregation of TDP-43 upon proteasome inhibition in cultured neurons. *PLoS ONE* **6**, e22850.

**Vellas, B., Pahor, M., Manini, T., Rooks, D., Guralnik, J. M., Morley, J., Studenski, S., Evans, W., Asbrand, C., Fariello, R. et al.** (2013). Designing pharmaceutical trials for sarcopenia in frail older adults: EU/US Task Force recommendations. *J. Nutr. Health Aging* **17**, 612-618.

**Watts, G. D., Wymer, J., Kovach, M. J., Mehta, S. G., Mumm, S., Darvish, D., Pestronk, A., Whyte, M. P. and Kimonis, V. E.** (2004). Inclusion body myopathy associated with Paget disease of bone and frontotemporal dementia is caused by mutant valosin-containing protein. *Nat. Genet.* **36**, 377-381.

**Weihl, C. C. and Pestronk, A.** (2010). Sporadic inclusion body myositis: possible pathogenesis inferred from biomarkers. *Curr. Opin. Neurol.* **23**, 482-488.

**Winder, S. J., Lipscomb, L., Angela Parkin, C. and Juusola, M.** (2011). The proteasomal inhibitor MG132 prevents muscular dystrophy in zebrafish. *PLoS Curr.* **3**, RRN1286.

**Yamashita, S., Kimura, E., Tawara, N., Sakaguchi, H., Nakama, T., Maeda, Y., Hirano, T., Uchino, M. and Ando, Y.** (2013). Optineurin is potentially associated with TDP-43 and involved in the pathogenesis of inclusion body myositis. *Neuropathol. Appl. Neurobiol.* **39**, 406-416.

**Zhao, J., Brault, J. J., Schild, A., Cao, P., Sandri, M., Schiaffino, S., Lecker, S. H. and Goldberg, A. L.** (2007). FoxO3 coordinately activates protein degradation by the autophagic/lysosomal and proteasomal pathways in atrophying muscle cells. *Cell Metab.* **6**, 472-483.

nature COMMUNICATIONS

ARTICLE

Received 26 Dec 2013 | Accepted 6 Feb 2014 | Published 6 Mar 2014

DOI: 10.1038/ncomms4396

# Quantitative live-cell imaging reveals spatio-temporal dynamics and cytoplasmic assembly of the 26S proteasome

Chan-Gi Pack[1], Haruka Yukii[2], Akio Toh-e[3], Tai Kudo[2], Hikaru Tsuchiya[2], Ai Kaiho[2], Eri Sakata[4], Shigeo Murata[5], Hideyoshi Yokosawa[6], Yasushi Sako[1], Wolfgang Baumeister[4], Keiji Tanaka[2] & Yasushi Saeki[2]

The 26S proteasome is a 2.5-MDa multisubunit protease complex that degrades polyubiquitylated proteins. Although its functions and structure have been extensively characterized, little is known about its dynamics in living cells. Here, we investigate the absolute concentration, spatio-temporal dynamics and complex formation of the proteasome in living cells using fluorescence correlation spectroscopy. We find that the 26S proteasome complex is highly mobile, and that almost all proteasome subunits throughout the cell are stably incorporated into 26S proteasomes. The interaction between 19S and 20S particles is stable even in an importin-α mutant, suggesting that the 26S proteasome is assembled in the cytoplasm. Furthermore, a genetically stabilized 26S proteasome mutant is able to enter the nucleus. These results suggest that the 26S proteasome completes its assembly process in the cytoplasm and translocates into the nucleus through the nuclear pore complex as a holoenzyme.

[1] Cellular Informatics Laboratory, RIKEN, 2-1 Hirosawa, Wako, Saitama 351-0198, Japan. [2] Laboratory of Protein Metabolism, Tokyo Metropolitan Institute of Medical Science, Setagaya-ku, Tokyo 156-8506, Japan. [3] Medical Mycology Center, Chiba University, 1-8-1 Inohana, Chiba 260-8673, Japan. [4] Department of Molecular Structural Biology, Max-Planck-Institute of Biochemistry, 82152 Martinsried, Germany. [5] Laboratory of Protein Metabolism, Graduate School of Pharmaceutical Sciences, the University of Tokyo, 7-3-1 Hongo, Bunkyo-ku, Tokyo 113-0033, Japan. [6] Department of Medicinal Biochemistry, School of Pharmacy, Aichi Gakuin University, 1-100 Kusumoto-cho, Chikusa-ku, Nagoya 464-8650, Japan. Correspondence and requests for materials should be addressed to Y.S. (email: saeki-ys@igakuken.or.jp).



© 2014 Macmillan Publishers Limited. All rights reserved.

The 26S proteasome is a multisubunit protease that degrades polyubiquitinated proteins in an ATP-dependent manner[1–3]. It is involved in a wide variety of cellular processes, and proteasomal dysfunctions lead to a variety of diseases[4]. The 26S proteasome is composed of at least 33 different subunits, organized into two particles: a highly conserved 20S core particle (CP), containing the central catalytic cavity, and one or two 19S regulatory particles (RPs). The CP is a barrel-shaped structure of ~730 kDa, consisting of four heptameric rings, whereas the RP is a ~930-kDa complex consisting of 19 different subunits. The RP mediates multiple aspects of proteasome function such as recognition, deubiquitylation and unfolding of substrates and translocation of substrates into the CP. The RP can be separated into two major subcomplexes, the base and the lid[3]. The base includes six different AAA + ATPase subunits (Rpt1–6) and three non-ATPase subunits (Rpn1, 2 and 13), whereas the lid consists of nine non-ATPase subunits (Rpn3, 5–9, 11, 12 and 15). The lid partially surrounds the ATPase ring of the base, and two ubiquitin receptors, Rpn10 and Rpn13, are located on the periphery of the 19S RP[5–8]. Recent studies have suggested that the assembly of the proteasome proceeds via a highly ordered multistep mechanism[9–12]. All of the subcomplexes of the proteasome (CP, base, and lid) seem to assemble independently; the CP and base require multiple proteasome-dedicated chaperones for efficient and correct assembly.

In proliferating yeast and some cultured mammalian cells, the 26S proteasome is highly enriched in the nucleus, where it is involved in degradation of nuclear proteins[13–17]. Because only a small number of proteasome subunits contain a nuclear localization signal (NLS)[13,18,19], and because yeast undergoes a closed mitosis in which the nuclear envelope remains intact and mitosis occurs within the nucleus, the yeast proteasome must enter the nucleus in an at least partially assembled form. In support of this notion, previous studies have shown that CP components are imported into the nucleus as inactive precursor complexes via the importin-α/β pathway[20]. Additional evidence suggests that the CP and the lid and base subcomplexes are imported separately[19,21]. These observations imply that the yeast 26S proteasome is assembled inside the nucleus from independently imported modules. By contrast, other studies have suggested that the holoenzyme or novel form of the preassembled proteasome undergoes nuclear translocation[22–24]. Because the channel of the nuclear pore complex (NPC) can expand to accommodate cargoes with a diameter of up to 39 nm, as revealed by studies using gold particles[25], it is theoretically possible for intact CP or even the entire 26S proteasome to pass through the NPC. However, the inner channel of the NPC is largely composed of unstructured FG-repeat-containing nucleoporins that create a hydrophobic meshwork that acts as a permeability barrier[26], potentially preventing the translocation of the proteasome. Therefore, it remains unclear whether the intact 26S proteasome can pass through the NPC.

In this study, we investigated the absolute concentration, dynamics, and complex formation of the 26S proteasome in living yeast cells by fluorescence correlation spectroscopy (FCS)[27–30], a method for quantitative live-cell imaging. Unexpectedly, we found that the 26S proteasome is a highly mobile complex, and that almost all proteasome subunits are stably incorporated into 26S proteasomes in both the cytosol and nucleus. Complex formation is not significantly altered in an importin-α mutant, suggesting that the proteasome is assembled in the cytosol. Consistent with this, a genetically stabilized 26S proteasome in which the RP and CP are fused does not exhibit any obvious defects and is distributed normally in the nucleus. These results suggest that the 26S proteasome can complete its assembly process in the cytoplasm and translocate into the nucleus through the NPC as a holoenzyme.

## Results

**Dynamics of the 26S proteasome revealed by FCS.** FCS[27–29] measures fluorescence fluctuations within a defined volume, determined by the laser and the optical setup, to determine a correlation function for probe molecules (Fig. 1). Fitting of mathematical models of the fluorescence correlation function (FCF) allows determination of the concentration of the target complex, as well as its the diffusion coefficient ($D$), which is directly related to molecular weight and shape (Fig. 1). We first investigated whether these methods could be applied to macromolecules in extracts from cells expressing chromosomally green fluorescent protein (GFP)-tagged proteasome subunit (Pre6)[14,21], Hsp104, or ribosome subunit Rpl19a (Fig. 2)[31–33]. All of the FCF curves fit well to a one-component diffusion model (Fig. 2), suggesting that each of these macromolecules were present as a single entity in the extract. The molecular weights ($MW_{fcs}$) estimated from the measured $D$ values for Hsp104 and the proteasome were larger than their theoretical molecular weights (Table 1). However, this inconsistency can be explained by a model using standard spherical particles (Supplementary Fig. 1a) that takes into account the shapes of Hsp104 and the proteasome, including the presence of cavities in these complexes (Supplementary Fig. 1b–d).

We next applied FCS to living yeast cells (Fig. 3; Supplementary Fig. 2). To elucidate the dynamics of all subcomplexes of the proteasome at their endogenous expression levels, we studied yeast cells expressing chromosomally GFP-tagged Pre6 (a CP subunit), Rpn1 (a base subunit) or Rpn7 (a lid subunit) (Fig. 3a). Exponentially growing cells were mounted on a glass-bottom dish to eliminate possible mechanical stress[34]. We measured proteasome dynamics in both the cytoplasm and nucleus. The FCF curves in both compartments were very similar for all three subunits (Fig. 3b; Supplementary Fig. 3). Unexpectedly, the mobilities of the subunits in live cells had two or more components, rather than the simple one-component diffusion observed in extracts. Because a two-component diffusional model fitted well to the FCF curves (see Methods), we conclude that almost all proteasome subunits exist within cells as components of two species. Based on our previous finding that the apparent viscosity in the yeast cell is ~4 cP (ref. 31), we calculated that the size of one of these species (represented by $D_{fast}$) is 1–10 MDa, whereas the size of the other (represented by $D_{slow}$) is ~32 GDa (Table 2). The smaller species seemed to represent the bona fide 26S proteasome (Supplementary Fig. 4), whereas the larger species seemed to represent a novel form of the proteasome, possibly reflecting strong interactions with other cellular components. From the initial amplitude of the correlation curve, $G(0)$, we calculated the absolute concentrations of the proteasome subunits: 140–200 nM in the cytoplasm and 830–980 nM in the nucleus (Fig. 3c).

As a control for our *in vivo* measurements of proteasome dynamics, we analysed a mutant of Rpn2, the second largest subunit of the proteasome, in which proteasome assembly is defective. In the *rpn2* mutant, the 26S proteasome was almost completely disassembled into the lid, base (lacking Rpn2) and CP even at the permissive temperature[21]. Indeed, the FCF curves of Pre6-GFP, Rpn1-GFP and Rpn7-GFP were dramatically altered (Fig. 3d and Table 2). $D_{fast}$ values for Pre6-GFP, Rpn1-GFP and Rpn7-GFP were twofold larger than in wild-type cells, indicating ~8-fold reductions of their $MW_{fcs}$. This experiment illustrates that dissociation of the holo-proteasome into its constituent


© 2014 Macmillan Publishers Limited. All rights reserved.

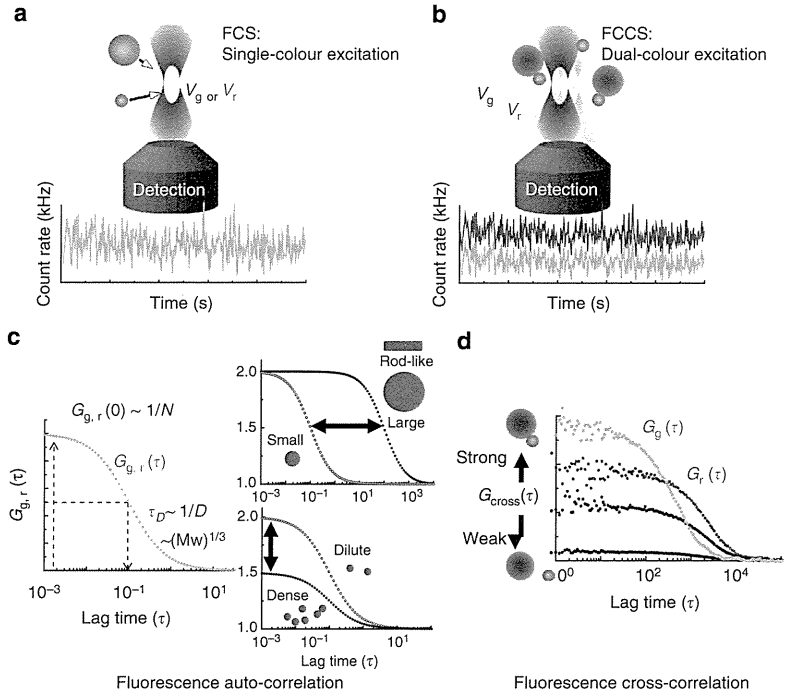


**Figure 1 | Schematic diagram for FCS and FCCS setup and parameters.** (**a**) One-color fluorescence auto-correlation (FCS) and (**b**) dual-color cross-correlation spectroscopy (FCCS) are methods based on fluctuation analysis of fluorescence intensity (count rate or c.p.s., kHz) detected from a tiny open volume ($V_g$ or $V_r$ for FCS, $V_g$ and $V_r$ for FCCS). Subscripts g and r represent green and red fluorescent probes, respectively. (**c**) FCS provides a fluorescence auto-correlation function ($G_g$ or $G_r$), allowing measurement of two important biophysical parameters: the average number of fluorescent molecules ($N$) in a detection volume and the translational diffusion time ($\tau_D$) of the molecules through the open volume. Mobility parameter ($\tau_D$ or $D$) of molecules reflects the molecular size (MW or $R_h$), shape of fluorescent species, and the apparent viscosity in solution or in a live cell (see also Methods). (**d**) Dual-color FCCS provides a cross-correlation function ($G_{cross}$, represented by $G_c$ in the main text) and two auto-correlation functions ($G_g$ and $G_r$), respectively. $G_c$ allows measurement of direct interaction or colocalization of a green and red fluorescent molecules transiting through open volumes $V_g$ and $V_r$, in addition to the parameters for one-color FCS as described in **c**.

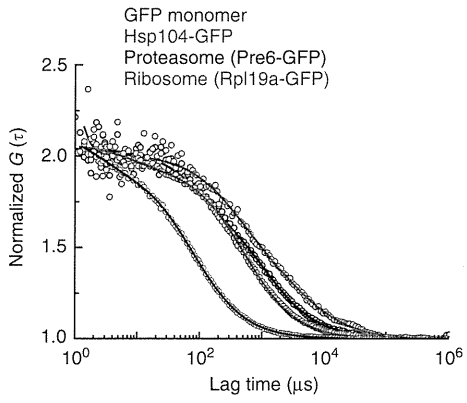


**Figure 2 | Quantitation by FCS of GFP-tagged macromolecules in extracts.** FCS analysis of the proteasome and giant protein complexes in yeast lysates. Extracts from cells expressing monomeric GFP (YCP001), Hsp104-GFP (YCP003), Pre6-GFP (YYS1033) or Rpl19a-GFP (YCP004) were analysed by FCS. Representative normalized FCF curves of different sizes of proteins are shown (circle symbol). For comparison of mobility, all of the curves were normalized to the same amplitude, $G(0) = 2$. Solid lines indicate fitting of one-component models to the results.

subcomplexes can be monitored by FCS analysis, and that FCS analysis can be applied to the *in vivo* measurement of proteasome dynamics.

Next, we sought to characterize the slower-mobility species with an apparent molecular weight of ~32 GDa. We hypothesized that the very slow correlation might reflect binding and unbinding to immobile cellular components. The fractional ratios of $D_{fast}$ and $D_{slow}$ differed slightly between the cytosol and the nucleus, but overall ~40% of total proteasomes in both compartments appeared to be associated with cellular components (Table 2; Supplementary Fig. 3). Notably, in *rpn2* cells, the fraction of the slower-mobility species decreased to ~20%, suggesting that fully assembled proteasomes, rather than constituent subcomplexes, associate with these cellular components. Recent studies suggested that cytoplasmic proteasomes interact directly with actin fibres[35], and that nuclear proteasomes associate with chromatin during the transcription process[36]. To test these ideas, we exposed cells to drugs targeting these features of the cell. Disruption of actin fibres by latrunculin A did not affect proteasome mobilities (Supplementary Fig. 5a,b), suggesting that the proteasomes do not associate with an intact actin cytoskeleton. By contrast, inhibition of RNA polymerase II by actinomycin D decreased the fraction of the slower-mobility proteasomes (Supplementary Fig. 5c), suggesting that a large fraction of proteasomes is engaged with actively transcribed chromatin in the nucleus. Further studies are needed to determine the proteasome-associated cellular components in the cytoplasm.



© 2014 Macmillan Publishers Limited. All rights reserved.

**Table 1 | Summary of calculated molecular weights (MW) and diffusion coefficients (*D*) of GFP-tagged macromolecules in extracts.**

| Proteins | GFP-tagged proteins | Theoretical MW | $D_{fcs}$ ($\mu m^2 s^{-1}$)* | $MW_{fcs}$ |
|---|---|---|---|---|
| Fluorescent proteins | GFP monomer, mCherry | $28 \times 10^3$ | $78 \pm 1.8$ | $25 \times 10^3$ |
| | Tandem 3XGFP (rod-like shape) | $85 \times 10^3$ | $43.2 \pm 1.4$ | $164 \times 10^3$ |
| Hsp104 | Hsp104-GFP (6 nm cavity) | $132 \times 10^3$ ($792 \times 10^3$)† | $12 \pm 1.0$ | $8.6 \times 10^6$ |
| 26S proteasome | Pre6-GFP (rod-like and small cavity) | $2.56 \times 10^6$ (26S + two GFP)‡ | $10 \pm 1.5$ | $10 \times 10^6$ |
| Ribosome | Rpl19a-GFP (diameter ~28 nm) | Unknown | $7.5 \pm 1.0$ | $28 \times 10^6$ |

*Diffusion coefficients (*D*) were calculated from the FCF fitting result (means ± s.d.; $n = 3$).
†MW of Hsp104-GFP as hexamer.
‡MW of the proteasome as double-capped 26S proteasome.

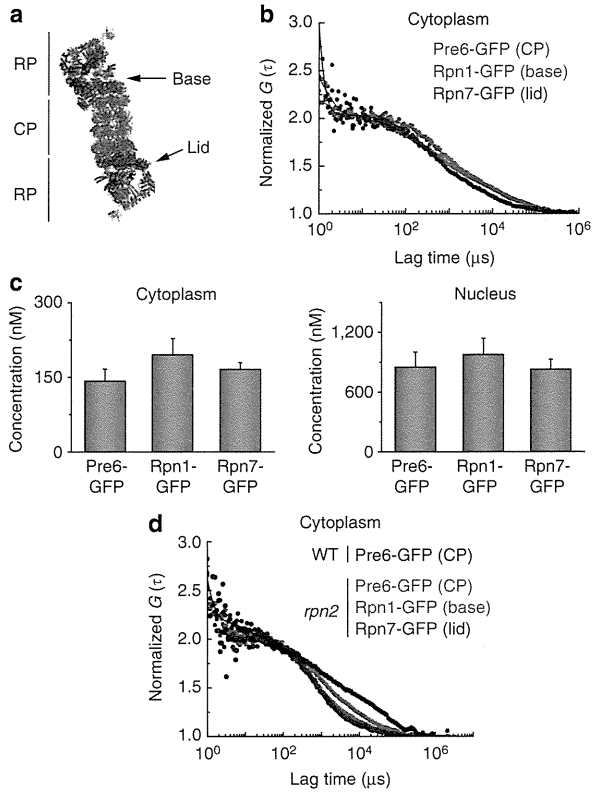


**Figure 3 | Quantitation by FCS of GFP-tagged proteasome subunits in living cells.** (**a**) The structure of the 26S proteasome adapted the atomic structural model (PDB ID: 4B4T). Subcomplexes of the proteasome are indicated: CP in green, base in red and lid in blue. (**b**) FCS analysis of proteasome subunits in living yeast cells. Normalized FCF curves are shown for Pre6-GFP (CP, YYS1033), Rpn1-GFP (base, YYS1034) and Rpn7-GFP (lid, YYS1035), measured in the cytoplasm. Solid lines indicate fitting of two-component models to the results. See Methods in detail. (**c**) Absolute concentrations of proteasome subunits in the cytoplasm and nucleus. The concentrations of proteasome subunits in living cells were calculated from measured FCFs (means ± s.e.m.; $n = 45$ cells). (**d**) FCS analysis of proteasome subunits in *rpn2* mutant cells. *rpn2* mutant cells expressing Pre6-GFP (CP, YYS2110), Rpn1-GFP (base, YYS2111), or Rpn7-GFP (lid, YYS2112) were analysed by FCS. Normalized FCF curves measured in the cytoplasm are shown. For comparison of mobility, all of the curves in **b** and **d** were normalized to the same amplitude, $G(0) = 2$. Solid lines indicate fitting of two-component model to the results.

**The 26S proteasome is a very stable complex in living cells.** Dual-color fluorescence cross-correlation spectrometry (FCCS) is designed to examine complex formation between two molecules labelled with different colours (e.g., GFP and mCherry, Fig. 1)[27–29]. The observations described above indicated that almost all proteasome subunits exist as the 26S proteasome. To confirm these findings, we carried out FCCS analysis in cells co-expressing Rpn7-GFP (lid) and Pre6-mCherry (CP) (Fig. 4a). If the lid subunit and the CP subunit exist in the same complex, we should observe co-diffusion of GFP and mCherry as they enter and leave the focal volume, represented by the amplitude of cross-correlation, $G_c(0)$[27–29]. As shown in Fig. 4b, high cross-correlation was indeed observed between Rpn7-GFP and Pre6-mCherry. The relative interaction amplitude between Rpn7-GFP and Pre6-mCherry, represented by $[G_c(0) - 1]/[G_{g\ or\ r}(0) - 1]$, was larger than that of a GFP–mCherry fusion protein, suggesting that the RP–CP interaction is quite strong (Fig. 4c). Notably, the same result was obtained in both the cytoplasm and nucleus. Thus, FCCS analysis revealed that the 26S proteasome is a very stable complex in live cells.

**The 26S proteasome can form in the cytoplasm.** Our FCS analysis did not detect proteasome assembly intermediates in wild-type cells, probably because such intermediates are not abundant[37–40]. Previous studies using a specific importin-α mutant, *srp1-49*, suggested that nucleocytoplasmic transport mediated by importin α/β is coupled to proteasome biogenesis[19–21,23]. We hypothesized that proteasome intermediates might be detected in the *srp1-49* mutant. To test this idea, we analysed proteasome dynamics in the *srp1-49* mutant by FCS/FCCS. As reported previously, when cultures of *srp1-49* cells were shifted to the restrictive temperature for 6 h, corresponding to four doubling times, newly synthesized proteasome subunits were retained in the cytoplasm and accumulated at the outer membrane of the nuclear envelope[21] (Fig. 5a). Under these conditions, we determined the absolute concentrations of the proteasome subunits. In *srp1-49* cells, the concentration of each subunit was increased 2-fold in the cytoplasm relative to the concentration in wild-type cells, whereas the nuclear concentrations were decreased threefold (Fig. 5b). Unexpectedly, we did not detect assembly intermediates or free subcomplexes in *srp1-49* cells by FCS. This observation raised the possibility that the proteasome is assembled in the cytoplasm. To monitor the assembly status of the proteasome complex, we constructed an *srp1-49 RPN7-GFP PRE6-mCherry* strain and analysed it by FCCS. The relative cross-correlation amplitudes between Rpn7-GFP and Pre6-mCherry did not change over 3 or 6 h of culture (two or four doublings, respectively) at the restrictive temperature (Fig. 5c). Accordingly, the interaction amplitudes changed only slightly in both the cytoplasm and the nucleus (Fig. 5d). These


© 2014 Macmillan Publishers Limited. All rights reserved.

**Table 2 | Comparisons of the proteasome mobility between wild-type and *rpn2* cells.**

| | Wild type | | *rpn2* | |
|---|---|---|---|---|
| **GFP-tagged proteins** | $D_{fast}$ ($\mu m^2 s^{-1}$)* (%)† | $D_{slow}$ ($\mu m^2 s^{-1}$)* (%) | $D_{fast}$ ($\mu m^2 s^{-1}$)* (%)† | $D_{slow}$ ($\mu m^2 s^{-1}$)* (%) |
| Pre6 (CP) | 6.0 ± 0.35 (55) | 0.25 ± 0.01 (45) | 11.3 ± 0.30 (73) | 0.7 ± 0.10 (27) |
| Rpn1 (base) | 6.0 ± 0.51 (53) | 0.31 ± 0.03 (47) | 12.1 ± 0.34 (80) | 1.0 ± 0.14 (20) |
| Rpn7 (lid) | 5.3 ± 0.48 (59) | 0.31 ± 0.03 (41) | 12.0 ± 0.50 (81) | 1.3 ± 0.20 (19) |
| GFP monomer (control)‡ | 21.6 ± 0.7 (93) | 0.2 ± 0.1 (7) | | |

*Diffusion coefficients ($D$: $D_{fast}$, $D_{slow}$) were calculated from the FCF fitting result (means ± s.e.m.; $n = 45$ for WT and $n = 20$ for *rpn2* mutant).
†Fractional ratios, $F_{fast}$ and $F_{slow}$ of $D_{fast}$ and $D_{slow}$ are represented by percentage.
‡Diffusion of GFP monomer in live yeast cells is shown as a reference.

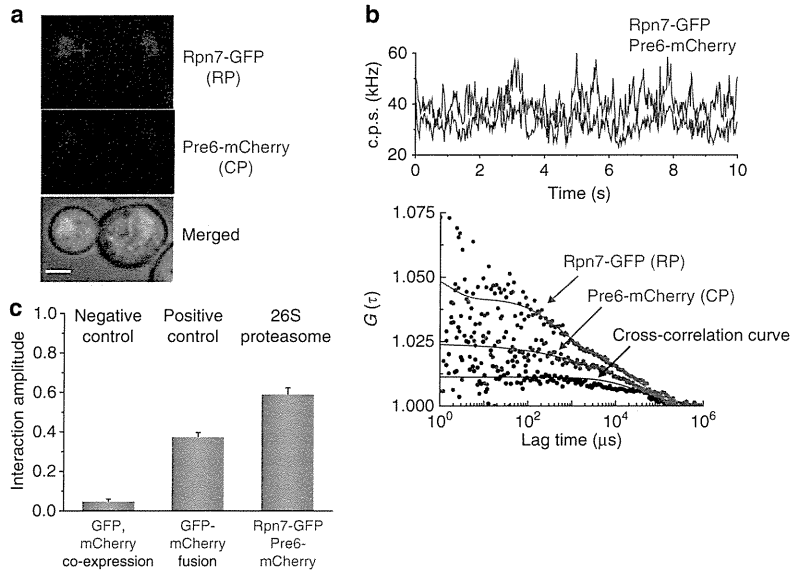


**Figure 4 | Stable complex formation of the 26S proteasome in living cells.** (**a**) Fluorescence-microscopic image of *RPN7-GFP PRE6-mCherry* cells (YYS1163). Scale bar, 2 μm. (**b**) Representative FCCS measurement of the *RPN7-GFP PRE6-mCherry* cells. (Upper) Change over time of average fluorescence intensity (counts per second; cps in kHz). (Bottom) Two corresponding FCFs (green and red) and one FCCS curve (black) indicate a strong interaction. (**c**) Summary of interaction amplitude of the RP–CP interaction. Interaction amplitude represents the mean value of the relative cross-correlation amplitude. As controls, cells co-expressing GFP and mCherry protein (negative control, YCP002) or GFP–mCherry fusion protein (positive control, YYS1419) were also analyzed (means ± s.e.m.; $n = 15$).

results suggest that the 26S proteasome was still able to form in the cytoplasm even when nuclear import is impaired.

To rule out the possibility that cytoplasmic accumulation of the subcomplexes artificially induced formation of 26S proteasomes, we deleted *RPN4* from *srp1-49* cells. Rpn4 is a transcription factor that regulates proteasome concentrations; deletion of *RPN4* significantly reduces the levels of proteasome subunits[39,41]. Consistent with this, the cytoplasmic concentration of Rpn7-GFP, measured by FCS, decreased to ~160 nM in *srp1-49 rpn4Δ* double-mutant cells at both the permissive and non-permissive temperatures (Supplementary Fig. 6). Next, we analysed these cells by FCCS. Although the interaction amplitude between Rpn7-GFP and Pre6-mCherry in the *srp1-49 rpn4Δ* mutant was slightly lower than that in wild-type cells, it did not change at the non-permissive temperature. Thus, 26S proteasomes could still form in *srp1-49 rpn4Δ* mutant cells. Together, these results suggest that nuclear import is not required for the formation of the 26S proteasome.

**Stabilized holoproteasomes are localized in the nucleus.** Our results obtained from live-cell measurements demonstrate that the 26S proteasome can form in the cytoplasm, and then enter the nucleus. As noted above, the channel of the NPC can expand to 39 nm (ref. 25), the 26S proteasome could translocate into the nucleus through via the NPC. However, the inner channel of the NPC serves as a permeability barrier[26], which potentially prevents translocation of the 26S proteasome as intact complex. The 26S proteasome is intrinsically unstable: it is easily dissociated into the RP and the CP *in vitro*, and recent studies have also suggested that the RP–CP interface is structurally fragile on exposure to oxidative stress *in vivo*[42]. Because only a few proteasome subunits contain NLS sequences, dissociation might occur at the subcomplex level, especially at the RP–CP interface. In our FCCS measurements, the time resolution is limited to > 10 μs, therefore, the data described above cannot rule out the possibility that 26S proteasome undergo very fast dissociation and re-association during translocation through the NPC.

To rule out the possibility and show that the holo-complex can enter the NPC, we constructed a strain in which the RP and CP particles were fused: specifically, the CP subunit Pre6 (α4) was genetically fused to the RP subunit Rpt1 or Rpt2 (Fig. 6a). The RP-CP–fused strains exhibited wild-type growth even in the


© 2014 Macmillan Publishers Limited. All rights reserved.

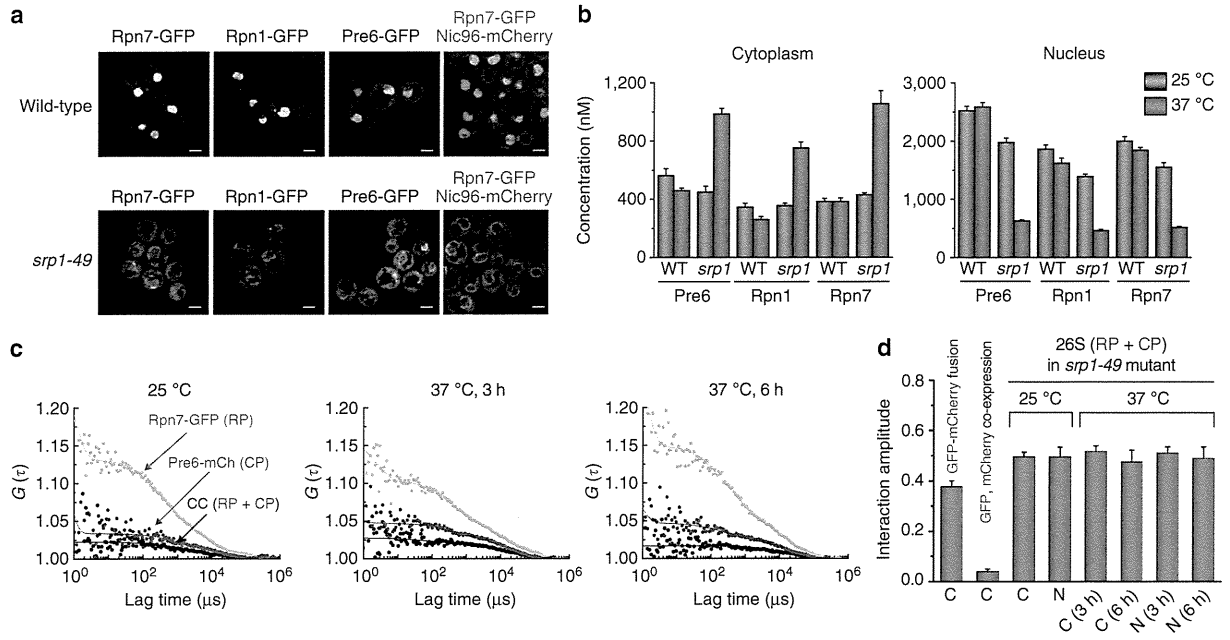


**Figure 5 | FCS and FCCS analyses of the proteasome in an importin-α mutant.** (**a**) Cytoplasmic accumulation of the proteasome subunit in an importin-α mutant. Wild-type or importin-α mutant (*srp1-49*) cells expressing GFP-tagged proteasome subunits (YSO11, 12, 33, 34, 47 and 52), and cells expressing mCherry-tagged Nic96, a component of the nuclear pore complex (YYS1969 and 1970), were cultured for 6 h at 37 °C (corresponding to four doubling times) and imaged by confocal microscopy. Scale bars, 2 μm. (**b**) Absolute concentrations of proteasome subunits in *srp1-49* cells. The concentrations of the proteasome subunits in the cytoplasm and nucleus were determined at both permissive (25 °C) and restrictive (37 °C, 6 h) temperatures (means ± s.e.m.; $n=15$). (**c**) FCCS measurement of *srp1-49 RPN7-GFP PRE6-mCherry* cells. Representative FCCS curves from *srp1-49 RPN7-GFP PRE6-mCherry* cells (YYS1745) under the indicated conditions. CC, cross-correlation curve. (**d**) Summary of interaction amplitude of the RP-CP interaction in *srp1-49* mutant cells. Interaction amplitude, representing the mean value of the relative cross-correlation amplitude, was calculated from the correlation curves measured in live cells under each condition (means ± s.e.m.; $n=15$).

presence of oxidative stress (Fig. 6b). Because these subunits are essential, the genetic studies suggested that the fusion proteins were functional. Protein bands corresponding to the Rpt1–Pre6 and Rpt2–Pre6 fusion proteins could be detected in the corresponding lysates and in affinity-purified RP-CP–fused proteasomes (Fig. 6c; Supplementary Fig. 7). The RP–CP proteasome could be purified as the holo-complex even in the absence of ATP (Fig. 6c, right panel), suggesting that almost all proteasomes contained stoichiometric amounts of the fusion proteins. These observations support the CP template assembly model of the RP[39]. Furthermore, structural analysis by cryo-electron microscopy revealed that the Pre6-Rpt2–fused proteasome was almost indistinguishable from the wild-type proteasome (Fig. 6d). Thus, we concluded that the RP-CP–fused proteasomes were functional both *in vivo* and *in vitro*.

Using these strains, we analysed the subcellular distribution of the RP-CP–fused proteasome. As shown in Fig. 7a, proteasome subunits were distributed normally in the nucleus. Importantly, the diffusion properties of the proteasomes measured by FCS were indistinguishable between RP-CP–fused and wild-type cells (Supplementary Fig. 7c). Nevertheless, it remained possible that the RP-CP–fused proteasomes assembled in the nucleus. Therefore, we performed nuclear import assays on these proteasomes. In quiescent cells, proteasomes form cytoplasmic granule structures called proteasome storage granules (PSGs)[34]. On addition of fresh medium, PSGs rapidly disappear, and proteasomes re-enter the nucleus within a few minutes[34]. By exploiting this phenomenon, we investigated whether the RP-CP–fused proteasomes could re-enter the nucleus. Because of the low efficiency of PSG formation in our W303 background cells, we used respiration-deficient cells in which intracellular pH rapidly declines on carbon depletion, resulting in efficient formation of PSGs (to be published). Both wild-type and the *PRE6-RPT1*–fused cells formed PSGs after 48 h of culture. Strikingly, on the addition of fresh medium, PSGs in both strains rapidly disappeared, and the proteasomes mobilized into the nucleus with the same kinetics (Fig. 7b). Thus, RP-CP–fused proteasomes entered the nucleus through the NPC, indicating that dissociation into RP and CP is not required for nuclear import of the assembled proteasome. Taken together, these results suggest that the 26S proteasome can enter the nucleus as the holoenzyme.

## Discussion

In this study, we determined the local concentrations of the proteasome in living yeast cells, and characterized the formation of the proteasome complex, using a quantitative imaging method. Previous studies have demonstrated that the base, base-like complex, and RP function in transcription, independent of the proteolytic function of the proteasome, implying that the proteasome subcomplexes may have specific roles in cells[43–45]. However, our results suggest that the 26S proteasome is a very stable complex, and that free base, RP, and subunits are not present at detectable levels anywhere in the cell, at least under normal culture conditions. In line with our findings, a recent study showed that the transcriptionally relevant form is the canonical 26S proteasome[46].

In a widely accepted model, the precursors of both RP and CP are translocated independently into the nucleus, where they are


© 2014 Macmillan Publishers Limited. All rights reserved.